

## Accepted Manuscript

A geochemical study of the winonaites: Evidence for limited partial melting and constraints on the precursor composition

Alison C. Hunt, Gretchen K. Benedix, Samantha J. Hammond, Philip A. Bland, Mark Rehkämper, Katharina Kreissig, Stanislav Strekopytov

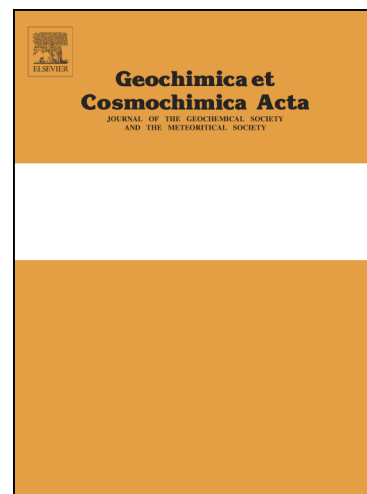
PII: S0016-7037(16)30621-4  
DOI: <http://dx.doi.org/10.1016/j.gca.2016.10.043>  
Reference: GCA 9998

To appear in: *Geochimica et Cosmochimica Acta*

Received Date: 3 May 2016  
Revised Date: 21 October 2016  
Accepted Date: 27 October 2016

Please cite this article as: Hunt, A.C., Benedix, G.K., Hammond, S.J., Bland, P.A., Rehkämper, M., Kreissig, K., Strekopytov, S., A geochemical study of the winonaites: Evidence for limited partial melting and constraints on the precursor composition, *Geochimica et Cosmochimica Acta* (2016), doi: <http://dx.doi.org/10.1016/j.gca.2016.10.043>

This is a PDF file of an unedited manuscript that has been accepted for publication. As a service to our customers we are providing this early version of the manuscript. The manuscript will undergo copyediting, typesetting, and review of the resulting proof before it is published in its final form. Please note that during the production process errors may be discovered which could affect the content, and all legal disclaimers that apply to the journal pertain.



**A geochemical study of the winonaites:  
Evidence for limited partial melting and constraints on the precursor  
composition**

Alison C. Hunt<sup>1\*</sup>, Gretchen K. Benedix<sup>2,3</sup>, Samantha J. Hammond<sup>4</sup>, Philip A. Bland<sup>2,3</sup>, Mark  
Rehkämper<sup>5</sup>, Katharina Kreissig<sup>5</sup>, Stanislav Strekopytov<sup>6</sup>

<sup>1</sup> The Natural History Museum, Earth Sciences, Cromwell Road, London, SW7 5BD, UK

<sup>2</sup>Department of Applied Geology, Curtin University, GPO Box U1987, Perth, WA 6845,  
Australia

<sup>3</sup>Department of Earth and Planetary Sciences, Western Australian Museum, Locked Bag 49  
Welshpool DC, Western Australia 6986, Australia.

<sup>4</sup>Department of Environment, Earth and Ecosystems, The Open University, Walton Hall,  
Milton Keynes, MK7 6AA, UK

<sup>5</sup>IARC, Imperial College London, Department of Earth Science and Engineering, South  
Kensington Campus, London SW7 2AZ, UK.

<sup>6</sup>The Natural History Museum, Imaging and Analysis Centre, Cromwell Road, London, SW7  
5BD, UK.

\*Corresponding author: [alison.hunt@erdw.ethz.ch](mailto:alison.hunt@erdw.ethz.ch); +41 (0)44 632 4643; +41 (0)44 632

1376 (fax). Now at: Institute of Geochemistry and Petrology, ETH Zürich, Clausiusstrasse 25,

8092 Zürich, Switzerland

ACCEPTED MANUSCRIPT

**Abstract**

The winonaites are primitive achondrites which are associated with the IAB iron meteorites. Textural evidence implies heating to at least the Fe, Ni-FeS cotectic, but previous geochemical studies are ambiguous about the extent of silicate melting in these samples. Oxygen isotope evidence indicates that the precursor material may be related to the carbonaceous chondrites. Here we analysed a suite of winonaites for modal mineralogy and bulk major- and trace-element chemistry in order to assess the extent of thermal processing as well as constrain the precursor composition of the winonaite-IAB parent asteroid.

Modal mineralogy and geochemical data are presented for eight winonaites. Textural analysis reveals that, for our sub-set of samples, all except the most primitive winonaite (Northwest Africa 1463) reached the Fe, Ni-FeS cotectic. However, only one (Tierra Blanca) shows geochemical evidence for silicate melting processes. Tierra Blanca is interpreted as a residue of small-degree silicate melting. Our sample of Winona shows geochemical evidence for extensive terrestrial weathering. All other winonaites studied here (Fortuna, Queen Alexander Range 94535, Hammadah al Hamra 193, Pontlyfni and NWA 1463) have chondritic major-element ratios and flat CI-normalised bulk rare-earth element patterns, suggesting that most of the winonaites did not reach the silicate melting temperature. The majority of winonaites were therefore heated to a narrow temperature range of between ~1220 (the Fe, Ni-FeS cotectic temperature) and ~1370 K (the basaltic partial melting temperature). Silicate inclusions in the IAB irons demonstrate partial melting did occur in some parts of the parent body (Ruzicka and Hutson, 2010), thereby implying heterogeneous heat distribution within this asteroid. Together, this indicates that melting was the result of internal heating by short-lived radionuclides. The brecciated nature of the winonaites suggests that the parent body was later disrupted by a catastrophic impact, which allowed the preservation of the largely unmelted winonaites.

Despite major-element similarities to both ordinary and enstatite chondrites, trace-element analysis suggests the winonaite parent body had a carbonaceous chondrite-like precursor composition. The parent body of the winonaites was volatile-depleted relative to CI, but enriched compared to the other carbonaceous classes. The closest match are the CM chondrites, however, the specific precursor is not sampled in current meteorite collections.

ACCEPTED MANUSCRIPT

## 1. Introduction

Primitive achondrite meteorites exhibit affinities with both chondrites and achondrites. They are characterised by mineral assemblages and bulk element compositions which resemble their chondritic precursors, but have textures that vary from high-grade metamorphic to those indicative of partial melting processes (e.g., Benedix et al., 1998; Weisburg et al., 2006). Currently, meteorite groups classified as primitive achondrites include the acapulcoites, lodranites, brachinites, and winonaites.

The winonaites are primitive achondrites with 29 individual samples (<http://www.lpi.usra.edu/meteor/metbull.php>, accessed 31/03/2016). They are related to silicate inclusions in IAB iron meteorites via their mineralogy, chemistry and oxygen isotope compositions (Bild, 1977; Clayton et al., 1983; Clayton and Mayeda, 1996; Benedix et al., 2000). Three criteria are typically used to classify the winonaites: (1) a highly reduced mineralogy (i.e. olivine typically  $Fa_{1-9}$ ; Benedix et al., 1998), (2) an oxygen isotopic composition within the range  $\Delta^{17}O = -0.40$  to  $-0.73$  ‰ (Clayton and Mayeda, 1996; Greenwood et al., 2012) and (3) a relatively high content of Fe-Ni metal and troilite relative to chondrites (up to 12.5 and 19.9 vol%, respectively; Benedix et al., 1998). Hypotheses for the origin of the winonaite-IAB parent body include: 1) localized impact melt pools, where the IAB irons are the result of several distinct impact events (Wasson et al., 1980; Choi et al., 1995; Wasson and Kallemeyn, 2002); 2) incomplete differentiation (Kelly and Larimer, 1977; Takeda et al., 1994; Takeda, 2000); and 3) incomplete differentiation followed by catastrophic impact break-up and reassembly (Benedix et al., 2000).

Winonaite textures imply varying degrees of planetary processing and brecciation. Iron-nickel metal and troilite are often present as veins cross-cutting silicate portions and are indicative of migration of a partial melt generated at the Fe, Ni – FeS cotectic (1223 K; Kullerud, 1963). Additionally, winonaites are characterised by heterogeneous grain-size and modal mineralogy, with some (i.e., Winona and Mt Morris, Wisc.) containing coarse-grained

olivine-rich areas which may represent the residues of large degrees of melting, while others (i.e., Pontlyfni) contain fine-grained areas enriched in plagioclase and high-Ca pyroxene that have been suggested to represent pockets of crystallised basaltic melt (Benedix et al., 1998). Variable whole-rock rare earth element (REE) abundances and patterns for samples including Winona and Mt Morris have also led some authors to suggest that limited partial melting and fractionation has occurred (e.g., Prinz et al., 1980). Alternatively, the winonaites and IAB silicate inclusions have also been interpreted as the residues of partial melting based on their chondritic FeO-MgO-MnO systematics (Goodrich and Delaney, 2000), while major- and trace-element data also suggest that the winonaites are in fact surprisingly similar to CI chondrites (Goodrich and Delaney, 2000; Floss et al., 2008). Any partial melting that has occurred on the winonaite-IAB parent body appears to have been limited (i.e., Benedix et al., 1998; Takeda et al., 2000; Benedix et al., 2005; Floss et al., 2008). As such, the winonaites can provide valuable insight into early asteroidal processes such as differentiation.

Previous studies have focussed on interpreting the thermal evolution of the winonaite parent body via trace element studies of individual minerals (i.e., Floss et al., 2008). Bulk data are only available for a few meteorites, and few elements overlap between different studies (Davis et al., 1977; Graham et al., 1977; Prinz et al., 1980, 1983). Furthermore, these studies often do not include analyses of the most volatile trace-elements, nor do they fully address the heterogeneous modal mineralogy of these samples. Here, we present modal mineralogy combined with bulk geochemical data for eight winonaites. This investigation aims to use this comprehensive geochemical dataset to explore the precursor composition of the winonaites and further understand the thermal evolution of the winonaite-IAB parent asteroid.

## **2. Samples and Analytical Methods**

Fourteen polished thin sections (PTS) of seven winonaites were examined in transmitted and reflected light, before analysis by scanning electron microscope (SEM) at the Natural History Museum, London (NHM) (Table 1). The majority of sections (12) were analysed

using a Zeiss Evo LS15 SEM operated at 20 kV and 5 nA beam current. Pontlyfni (M 6.1) and QUE 94535 were analysed using a LEO 1455VP SEM operated at 20 kV with a spot size of 500  $\mu\text{m}$  (roughly equivalent to a 2 to 5 nA beam current). All sections were scanned at 200 - 300x magnification, which is equivalent to roughly 2  $\mu\text{m}/\text{pixel}$  depending on the instrument. Images of each section were acquired as tiles for later montaging and therefore mapped with a ~50 pixel overlap between images. X-ray elemental maps were collected and automatically stitched together using the Oxford Instruments INCA software package. Maps were then processed to identify mineral phases and determine the modal abundances of major and minor phases in each sample using Adobe Photoshop, similar to the method described by Yugami et al. (1998) and Ford et al. (2008). Each section is analysed for modal abundance 5 times and an average is calculated from these data. The standard deviation of these 5 measurements is better than 1.7 % in all cases. Where it is possible to directly compare mineral modes for the same sections, we find good agreement with published literature. Comparisons of modal mineralogies can be made with the point-counting data of Benedix et al. (1998). Troilite abundances agree to better than 3 %, and often agree within our quoted standard deviation. Although Benedix et al. (1998) did not distinguish individual mafic minerals (olivine, low-Ca pyroxene, calcic-pyroxene, and phosphate), we add these minerals together in our new dataset to enable a comparison with the previous results. Our values for total abundance of mafic minerals are always lower than those reported by Benedix et al. (1998), and the biggest variations occur in the most weathered samples, Winona and Mt. Morris (Wisc.). This is likely to be an artefact of region picking, as our modal analyses include the weathered outer parts of these sections. There is greater variation between the two datasets for plagioclase abundance, with the point counting method Benedix et al. (1998) consistently recording a lower modal abundance except in one case. This is likely due to the subjective nature of point counting and the only subtle difference between mafic minerals and plagioclase in reflected light microscopy.

Seven winonaites were analysed for bulk major-element chemistry (Winona, Fortuna, Queen Alexander Range (QUE) 94535, Northwest Africa (NWA) 1463, Pontlyfni, Tierra Blanca and Hammadah al Hamra (HaH) 193; Table 1). Additionally, Winona, Fortuna, HaH 193 and QUE 94535 were analysed for their bulk trace-element chemistry. Full geochemical analyses can be conducted on <100 mg of powder; however, as the winonaites are extremely heterogeneous samples, larger chips (between 200 and 500 mg in total) were crushed in order to average out variations between pieces of the same sample (Hunt et al., 2011). Fusion crusts and weathered edges were removed from samples before powdering the whole rock by hand using an agate pestle and mortar.

Crushed samples were prepared for analysis by inductively coupled plasma atomic emission spectroscopy (ICP-AES) at the NHM to determine major and some minor elements. Elements analysed by ICP-AES for this study include Mg, Al, Si, Ca, Ti, Mn, Cr, Ni and Fe. Major element chemistry was determined by fusing  $\geq 40$  mg of sample with lithium metaborate ( $\text{LiBO}_2$ ) flux in a ratio of 1:3 and dissolving the resultant glass bead in  $\sim 0.8$  M nitric acid, before analysis with a Varian Vista Pro ICP-AES. The external reproducibility (RSD) for this dataset is better than 10 % except for Ni and FeO(t), based on repeat digestion and analysis of the H chondrites Ogi and Butsura. The higher external reproducibility for Ni and Fe (17 and 24 %, respectively) most likely reflects the heterogeneous distribution of Fe, Ni metal in the digested aliquots.

Minor and trace elements were analysed by inductively coupled plasma – mass spectrometry (ICP-MS) and include, among others, Sc, Ni, Sr, Zr, Ba, Pb, Th, U and the REE. Winona was digested at the Open University with a 3:1 concentrated  $\text{HNO}_3$ -HF mixture on a Teflon-coated hotplate in closed Savillex Teflon beakers. All other samples were digested in the clean room laboratories of the MAGIC (Mass Spectrometry and Isotope Geochemistry at Imperial College London) Research Centre at the Department of Earth Sciences and Engineering at Imperial College. Due to the presence of chromite in many winonaites, some

samples processed at Imperial College were treated using Parr bombs to ensure complete digestion. To this end, 50 mg of powdered sample were heated to 160 °C in a Parr bomb with ~ 1 ml of a 2:1 concentrated HF-HNO<sub>3</sub> mixture for >24 hours before drying down. Samples were then refluxed with aqua regia, followed by HNO<sub>3</sub>-HClO<sub>4</sub> in order to destroy any remaining material, including organics. Distilled acids were used throughout and blank concentrations for this procedure are negligible. Trace element concentrations were determined at The Open University using an Agilent 7500a ICP-MS. Samples were standardised against synthetic solutions and certified reference materials. These reference materials, along with repeat analyses of the H-chondrite Ogi, were used to assess external reproducibility. The precision of the ICP-MS measurements is better than 5 % (2 RSD) for all elements.

### 3. Results

#### 3.1 Modal mineralogy and textures

Modal abundances were determined for fourteen sections of seven different winonaite samples. Data are given as vol % in Table 2 and plotted on Figure 1. Additionally, the montaged element X-ray maps are available in the Electronic Annex (Figs. S1 – 14). The major silicate phases of the winonaites are low-calcium pyroxene, olivine, plagioclase feldspar and calcic pyroxene, which are present in approximately chondritic proportions (Benedix et al., 1998). They also contain abundant Fe, Ni-metal and troilite. Accessory phases can include amphibole, chromite, alabandite, daubreélite, schreibersite and apatite. Graphite has also been noted in the winonaites (Prinz et al., 1980; Benedix et al., 1998). Whilst these meteorites are extremely heterogeneous in terms of their modal mineralogy (Fig. 1), there are some similarities across the group, with low-Ca pyroxene being the dominant silicate in all samples except one, the unusual Winona BM 1930, 974. This is in contrast to ordinary chondrites, where olivine is dominant, and is consistent with formation under reducing

conditions relative to ordinary chondrites (McSween et al., 1991; Benedix et al., 2005).

However, the abundances of all phases varies greatly, even between different sections from the same meteorite.

Six sections of Winona were analysed as part of this study; three of these (USNM 854-1, UH 133, and UH 195) were previously examined by Benedix et al. (1998) and two (AMNH 4158-1 and 3768) were part of the initial study of primitive achondrites by Prinz et al. (1980). Of the sections studied, BM 1930, 974 exhibits an extreme departure in modal mineralogy from all other winonaites. This may in part be due to the smaller area of this thin section ( $\sim 16 \text{ mm}^2$ ) compared to the other Winona samples assessed here (at least  $80 \text{ mm}^2$ ; Table 2). In detail, BM 1930, 974 contains no low-Ca pyroxene, only 0.1 % olivine, and is comprised of abundant calcic pyroxene (9.7 %) and plagioclase (37.0 %), plus metal and troilite. Other sections of Winona generally show a medium-grained equigranular texture, with Fe, Ni-metal and troilite as interstitial grains and veins (Prinz et al., 1980; Benedix et al., 1998) (Fig. 2a). In sections UH 133 and UH 195 (which were cut from the same chip of meteorite), veins of troilite are up to 7.3 mm long and  $\sim 400 \mu\text{m}$  wide. These veins are often associated with schreibersite and subhedral chromite. Benedix et al. (1998) also note veins of up to 9 mm in length and  $100 \mu\text{m}$  width, comprising Fe, Ni-metal with troilite. Low-Ca pyroxene abundances vary from 21.2 to 41.6 % and olivine varies from 10.5 to 24.3 %. The amount of Fe, Ni-metal (including weathering products) varies from 16.9 to 48.6 %. The standard deviation about the mean Fe, Ni-metal abundance for all 6 samples of Winona is 14.5 %, highlighting the inherent heterogeneity of this meteorite. If the anomalous sample BM 1930, 974 is ignored, the standard deviation of plagioclase across the Winona sample-set is 4.1 %. The olivine/low-Ca pyroxene ratio is also highly variable, ranging from 0.49 in AMNH 3768 to 0.74 in AMNH 4158-1. Accessory phases in Winona include apatite (up to 0.7 %), chromite ( $\leq 0.1 \%$ ), schreibersite ( $\leq 0.1 \%$ , where present) and calcic pyroxene ( $\leq 0.5 \%$ ). These minor phases show variability in their abundances throughout Winona (Table 2).

Three thin-sections of Pontlyfni, the only fall among the winonaites, were assessed. Pontlyfni is more fine-grained than Winona, with an average grain size of 75  $\mu\text{m}$  (Benedix et al., 1998), although grain-size varies widely. The sections M 6.2 and M 6.3 have been previously studied by Benedix et al. (1998), and are re-examined here. They contain veins of Fe, Ni- metal, often associated or interspersed with schreibersite, up to 7 mm long and  $\sim 250$   $\mu\text{m}$  wide. All three sections show heterogeneously distributed Fe, Ni-metal and troilite, with PTS M 6.2 in particular characterised by often angular regions up to 2 mm across that are dominated by silicates (Fig. 2b). Troilite is particularly abundant in Pontlyfni (19.7 – 22.7 %), and in contrast with the other winonaites we have examined, it is more abundant than Fe, Ni-metal (9.8 – 15.3 %). As with Winona, and indeed all the winonaites, low-Ca pyroxene, olivine and plagioclase are the dominant silicate phases. The ratio of olivine to low-Ca pyroxene is lower for these samples compared to Winona, and ranges from 0.4 to 0.5. Accessory minerals present in Pontlyfni include calcic pyroxene (1.9 – 4.1 %) and schreibersite (0.6 – 1.3 %), plus minor amounts of daubreélite and alabandite. Pontlyfni exhibits a more restricted range of mineral modes than Winona, with a standard deviation across the three samples of less than 3.0 % for each mineral phase. However, unlike Winona, all three PTS of Pontlyfni were cut from the same chip of meteorite.

HaH 193 was previously examined by Floss et al. (2007), who recognised it as unique among the winonaites as it is the only sample which contains amphibole (fluoro-edenite; 1.4 %, this study). Amphibole poikilitically encloses small grains of olivine, plagioclase and calcic pyroxene, and most likely formed by reaction between calcic pyroxene and plagioclase (Floss et al., 2007). HaH 193 also contains large grains of low-Ca pyroxene that are up to 5 mm in length, and which poikilitically enclose olivine and plagioclase. Plagioclase has an abundance of 13.6 %, and the overall olivine/low-Ca pyroxene is 0.47. Iron-nickel metal and weathering products (26.6 %) are present as blebs and veins. Fine veins are extensive and pervasive throughout the section. A thicker, extensively weathered vein over 6 mm long and

up to 360  $\mu\text{m}$  wide cuts across the section and incorporates terrestrial material. Accessory minerals include minor chromite, apatite (0.1 %) and schreibersite (0.2 %).

Mount Morris (Wisc.), previously studied by Benedix et al. (1998), is generally medium-grained and equigranular. Metal is abundant (38.2 %, including weathering products), and is present as both small interstitial grains and large areas which reach over 4 mm in length. Schreibersite (0.7 %) is associated with these large regions. Mount Morris also contains Fe, Ni-metal as veins, although these are less abundant than in other samples. Its largest Fe, Ni-metal vein, over 11 mm long and up to 700  $\mu\text{m}$  wide, is extensively weathered and cuts across the section. Coarse grained olivine-rich regions (average grain-size 300 – 500  $\mu\text{m}$ ) have also been described in Mount Morris, as clumps and veins. In UH 157 these regions are often associated with metal veins (Benedix et al., 1998). The olivine/low-Ca pyroxene ratio (0.33) is similar to Pontlyfni, reflecting the generally lower olivine abundances of these samples. Plagioclase has an abundance of 15.5 % and accessory minerals present include chromite and calcic pyroxene (0.2 %).

Fortuna has an equigranular texture with abundant triple junctions and an average grain size of ~ 115  $\mu\text{m}$  (Russell et al., 2003). Troilite (7.1 %) and Fe, Ni-metal (7.7 %) are present as blebs and interstitial grains up to 600  $\mu\text{m}$  in size. Few Fe, Ni-metal veins are present in the section and the largest is ~ 5.8 mm long and up to 300  $\mu\text{m}$  wide. The olivine/low-Ca pyroxene ratio is 0.63, similar to many sections of Winona studied here (average 0.62). Plagioclase has an abundance of 16.3 % and numerous small grains of chromite (0.2 %) and apatite (0.3 %) are present in the section. Additionally, Fortuna contains more calcic pyroxene than all other meteorites analysed here (4.6 %), with the exception of the primitive winonaite NWA 1463, which has 8.7 % of this phase.

QUE 94535 is an Antarctic winonaite. It has a fine-grained texture similar to type-6 chondrites (Benedix et al., 1998). Troilite (6.6 %), schreibersite (0.7 %) and Fe, Ni-metal (9.8 %) are present as veins cross-cutting the section. Olivine/low-Ca pyroxene is 0.58, and

plagioclase feldspar and olivine abundances are 14.8 % and 24.0 %, respectively. Calcic pyroxene is present at 2.9 %, whilst other accessory minerals in QUE 94535 include daubreélite, alabandite and chromite.

NWA 1463 is one of the very few winonaites that contains relict chondrules. In addition, NWA 1463 lacks veins of Fe, Ni-metal and troilite and these phases are present exclusively as interstitial grains and blebs, which range up to ~ 1 mm in size. Small grains of metal are also seen rimming relict chondrules. The majority of NWA 1463 exhibits a recrystallized fine-grained texture, and resembles a type 5 chondrite (Floss et al., 2008). This has led to the suggestion that NWA 1463 is the most primitive of the winonaites (Benedix et al., 2003). Mineral modes in NWA 1463-3B are broadly consistent with the other winonaites, with abundant Fe, Ni-metal and troilite (16.0 and 8.9 %, respectively), and low-Ca pyroxene as the dominant silicate phase (49.0 %). However, NWA 1463 has the lowest olivine/low-Ca pyroxene ratio of any winonaite studied here (0.21). Relative to the other winonaites, NWA 1463 also has a high abundance of calcic pyroxene (8.7 %), but a low occurrence of plagioclase (6.4 %). Key accessory minerals in NWA 1463 are chromite (0.3 %), apatite (0.4 %) and schreibersite (0.1 %).

In addition to these samples, we analysed bulk material from a further winonaite, Tierra Blanca, and we briefly review the published modal mineralogy here. Tierra Blanca is among the coarsest-grained winonaites, with an average grain size of ~ 190  $\mu\text{m}$  and an equigranular texture (Floss et al., 2008). Thin sections of this meteorite indicate extensive weathering and alteration (Benedix et al., 1998; Floss et al., 2008). Tierra Blanca also contains large crystals of calcic pyroxene which are up to 9 mm in size and poikilitically enclose olivine, plagioclase and low-Ca pyroxene (Benedix et al., 1998; Floss et al., 2008; King et al., 1981). The olivine/low-Ca pyroxene ratio is 0.41 to 0.53 (Floss et al., 2008; King et al., 1981), consistent with the other winonaites examined in this work, and plagioclase has an estimated abundance between 6.3 and 14 % (Benedix et al., 1998; King et al., 1981).

### 3.2 Major element composition

Major and minor element concentrations for the seven winonaites are listed in Table 3. An initial comment concerns the low totals of these data, particularly for Winona, Tierra Blanca, HaH 193, and QUE 94535. There are several explanations for this observation. Primarily, S was not measured as part of this study. Sulfur concentration in the winonaites can range between 1.5 and 7.0 wt % (Graham et al., 1977; Jarosewich, 1990), and this missing element can largely explain the low totals. Additionally, three of our samples (Winona, Tierra Blanca, and HaH 193) are highly weathered, which may contribute to the low totals in two ways. Firstly, all Fe is calculated as  $\text{FeO}_{(t)}$ , but Fe may also be present in these samples as  $\text{Fe}_2\text{O}_3$ . This effect will be more pronounced for samples which have experienced higher degrees of weathering, as reduced Fe-metal breaks down oxidised phases. Secondly, the incorporation of  $\text{OH}^-$  and  $\text{H}_2\text{O}$  in weathering products will also contribute to our low totals. The major elements Si, Fe, and Mg show the greatest variability between the samples, with the largest variations seen in Winona. Our sample of Winona is most likely too weathered to give reliable results. It is also clear from the modal analysis (see above and Table 2) that Winona is very heterogeneous. We will largely exclude Winona from the discussion and interpretation of this dataset, but present our results in Tables 3 and 4 as only few published data are available for this sample.

In our new dataset (excluding Winona),  $\text{SiO}_2$  spans a range from 32 to 46 wt %. Magnesium oxide has a relatively restricted range (21 – 29 wt %), while  $\text{FeO}_{(t)}$  shows the widest range of concentrations (14 – 35 wt %). The latter two oxides are negatively correlated with each other. Interestingly, MgO is positively and  $\text{FeO}_{(t)}$  is negatively correlated with  $\text{SiO}_2$ , likely reflecting the varying amounts of metal in these samples. Similar patterns are seen for  $\text{Al}_2\text{O}_3$ , CaO and  $\text{Na}_2\text{O}$  for all samples, with Tierra Blanca having the lowest abundance of these elements. Although we have not determined the modal abundance of minerals in Tierra Blanca, Benedix et al. (1998) reported variable plagioclase abundances depending on thin

section. The phosphorus concentration is quite variable (0.2 to 0.4 wt %  $P_2O_5$ ), and is likely controlled by the abundance of apatite, which can also control the REE patterns (discussed below). There is a slight enrichment of Na in winonaites compared to most other chondritic meteorites, with the exception of EH chondrites. Chromium shows a bimodal distribution with a peak around ~ 900 ppm and a second at about 2700 ppm. QUE 94535 and HaH 193 have the lowest abundances of Cr, while Fortuna has the highest concentration. The Cr content does not correlate with modal abundance of chromite. There are number of possible explanations for this, including heterogeneity of the meteorite, incomplete dissolution of chromite in the bulk sample, or different redox conditions for the two groupings. However, Cr concentrations correlate positively with V. These two elements were determined using different digestion methods, and the fusion method in particular should result in complete digestion of the sample, including chromite. We therefore suggest that the measured Cr contents reflect the actual abundance in the aliquot of sample analysed, and are not an artefact of incomplete dissolution. This is an area of study for future work.

### ***3.3 Trace element composition***

The concentrations of 38 trace elements are listed in Table 4 for Winona, QUE 94535, HaH 193, and Fortuna. The CI-normalized lithophile element abundances of these meteorites are shown in Figure 3. QUE 94535, HaH 193 and Fortuna display broadly consistent trace-element patterns, whilst Winona is significantly different. A number of elements are either enriched or depleted relative to CI (Fig. 3). Notable enrichments are evident for Zr, Nb, and the light REE elements and are particularly strongly expressed in Winona. Depletions are evident in V, Zn, Rb and Cs. Amongst the chalcophile/siderophile elements (not plotted), Pd and Cu show depletions.

## **4. Discussion**

### ***4.1 Heterogeneity between the winonaites***

Based on the textures and modal mineralogy of the samples studied here (Table 2, Fig. 1 and 2), as well as previous investigations (Benedix et al., 1998; Floss et al. 2008), it appears that the winonaites are extremely heterogeneous. Standard deviations of mineral phases in the studied winonaites are given in the Electronic Annex (Table A1). For the samples studied here, low-Ca pyroxene abundance varies from 21 to 42 %, if anomalous Winona BM 1930, 974 (0 % low-Ca pyroxene) is excluded. Plagioclase feldspar contents vary from 6.4 to 25.9 % (again excluding BM 1930, 974), and total opaques (Fe, Ni metal, troilite, chromite, schreibersite, daubreélite, alabandite and associated weathering products) range from 15 to 53 %. This variability is also reflected in the textural diversity seen across the winonaites, and has resulted in long and varied thermal histories being proposed for these meteorites (i.e., Benedix et al., 2005; Benedix et al., 1998; Floss et al., 2008; Prinz et al., 1980; Yugami et al., 1998).

There is also a great deal of heterogeneity between different sections of the same sample. Variability in Winona ( $n = 6$ ) is much higher than the variability seen across the other winonaites. Total opaques range from 21 – 53 %, spanning nearly the entire range of winonaites studied here. Even when the anomalous BM 1930, 974 is excluded, the standard deviations across Winona for olivine, low-Ca pyroxene and plagioclase are 5.5 %, 7.6 % and 4.1 %, respectively. Texturally, these variations are expressed in a variety of ways. Iron-nickel metal in Winona ranges from thin veins plus blebs (i.e., AMNH 4158-1) to thick, pervasive veins with few obvious blebs (AMNH 3768-1). Silicate textures also range from recrystallized but broadly chondritic (i.e., UH 133), to coarse-grained regions dominated by olivine (USNM 854-1) that have previously been interpreted as melt residues (Benedix et al., 1998). Both modal mineralogy and texture support the idea that Winona has experienced a varied thermal history, with regions of different textures and therefore different thermal evolutions being juxtaposed together (Benedix et al., 2005; Benedix et al., 1998).

In Pontlyfni ( $n = 3$ ) this variability is less pronounced, and the standard deviation across the three sections for each mineral is no more than 3 %. These three sections also show similar textures and grainsizes, and all exhibit evidence for the mobilisation of Fe, Ni-FeS melts and metamorphism of silicates. Our three sections of Pontlyfni therefore have a very similar thermal history. However, in contrast to Winona, they were sampled from the same chip of meteorite and so it should not be surprising that they show less variability.

A consequence of the variable mineral modes and textures of the winonaites is that chemical analyses may reflect small-scale variations rather than the composition of the bulk meteorite. This may help elucidate localised thermal events, but will hinder the interpretation of body-wide evolution and composition. In order to reduce the effects of intra-sample heterogeneity, larger pieces of the winonaites were crushed (typically 200 – 500 mg) and an average bulk chemistry is shown in figures, where appropriate, to average out inter-sample heterogeneities.

#### **4.2 Thermal history of the winonaites**

The textural diversity seen in the winonaites implies a long and varied thermal history with several stages. Veins of Fe, Ni-metal and troilite indicate that all winonaites with the exception of NWA 1463 reached the Fe, Ni-FeS cotectic (1223 K; Kullerud, 1963). Comparison of winonaite textures to acapulcoites and lodranites implies that at least ~3 vol% partial melting affected these samples, with melting at the Fe, Ni-FeS cotectic only and no involvement of silicates (McCoy et al., 1997a). However, from textural evidence alone it is unclear whether the parent body also reached temperatures that were sufficiently high to initiate silicate melting.

Major-element data, however, can be used to distinguish between samples which have experienced silicate melting and those that have not. In particular, a plot of molar Mg/Si vs. Al/Si can be used to discriminate between unmelted material, silicate melt residues, and the

products of silicate melting. Figure 4a shows that most winonaites (excluding Winona, which is discussed in detail below) plot with ordinary chondrites, implying they have primitive compositions and do not record silicate melting. The majority of IAB silicate inclusions also plot in this field, whilst Tierra Blanca plots slightly away from the main group towards the field that represents melting residues. Two-pyroxene thermometry, which is likely to yield peak temperatures for these meteorites, gives a temperature of  $1473 \pm 100$  K for Tierra Blanca (Benedix et al., 1998). This is the highest temperature obtained for a winonaite and supports the inference that silicate melting affected this sample. Pontlyfni plots as primitive, unmelted material in Fig. 4a, despite previously being described as showing evidence of silicate melting (calcic-pyroxene-plagioclase enriched regions, Benedix et al., 1998). Additionally, two-pyroxene temperatures for Pontlyfni ( $1248 \pm 100$  K; Benedix et al., 1998) are too low to enable silicate melting. However, our bulk chemical data may be reconciled with silicate partial melting if the melt did not migrate on the scale of the meteorite chips sampled here.

Rare earth element data can also help elucidate whether silicate melting took place on the winonaite parent body. In general, CI-normalised REE concentrations for the winonaites, excluding Winona, show relatively flat patterns with some prominent exceptions (Fig. 5). Fortuna shows a slight positive Ce-anomaly, which is likely a result of terrestrial weathering (Floss and Crozaz, 1991), but otherwise displays a flat pattern. This suggests that Fortuna, QUE 94535 and HaH 193 either did not reach the silicate melting point or do not record melt migration, consistent with major-element data (Fig. 4a). Furthermore, a comparison with the melting models of Ruzicka and Hutson (2010) indicates that HaH 193, QUE 94535 and Fortuna cannot be modelled as either LREE-enriched melts or LREE-depleted melt residues, and are therefore unaltered by partial melting (Fig. 6). Data for two IAB silicate inclusions from Udei Station are also shown in Fig. 6 (Ruzicka and Hutson, 2010). Notably, these samples plot as residues (3B) or melts (1B), consistent with mineralogical evidence for melting among the IAB inclusions (Benedix et al., 2000). Based on H-chondrite melting

experiments, silicate partial melting in a chondritic system is thought to begin at  $\sim 1370$  K (Ford et al., 2008). The conclusion that the winonaites did not experience silicate melting is hence consistent with calculated two-pyroxene peak temperatures (1003 – 1473 K; Benedix et al., 1998), their textures (Benedix et al., 2005; Benedix et al., 1998; Floss et al., 2008; Floss et al., 2007; this study), and mineral chemistry (Floss et al., 2008). However, the Fe, Ni-metal textures of the winonaites suggest that the portion of the parent body sampled by these meteorites reached at least the Fe, Ni-FeS cotectic, allowing a narrow peak temperature range of about 1220 to 1370 K to be inferred for the winonaites.

Winona is exceptional compared to the other winonaites studied here. A previously analysed piece of Winona falls within the field of ordinary chondrites on a plot of molar Mg/Si vs. Al/Si (Mason and Jarosewich, 1967), which implies no silicate melting took place. However, previous REE analyses for Winona are highly variable. This may represent the heterogeneous distribution of phosphates and/or calcic pyroxene, but trace-element patterns for some pieces of Winona also indicate that igneous processes have affected this meteorite (Floss et al., 2008; Prinz et al., 1980). The piece of Winona studied here plots with the howardites and eucrites as it has higher molar Al/Si and lower molar Mg/Si compared to other Winona samples, and other winonaites (Fig. 4a). Howardites and eucrites are thought to originate from a single parent body, with a thermal history that is distinct from the winonaite-IAB parent in that it underwent large-scale differentiation and partial melting (i.e., Takeda, 1997). The howardites and eucrites are interpreted to represent partial melts (i.e., Stolper, 1977; Takeda, 1997), and our portion of Winona plots close to these samples in Fig. 4a, suggesting it may also have undergone silicate partial melting, albeit on a much smaller scale. The compositional differences between pieces of Winona are consistent with the textural heterogeneity and the range of temperatures inferred by two-pyroxene peak thermometry for this meteorite (1249 -1357 K; Benedix et al., 2005; Benedix et al., 1998). Based on this evidence, it is likely that some regions of Winona experienced silicate partial melting,

whereas others only reached the Fe-FeS cotectic melting point. New trace-element data for Winona record the highest REE concentration determined for a winonaite thus far and also reveal a negative Eu-anomaly (Fig. 5). However, unlike previous analyses of Winona, our new results also show a positive Ce-anomaly. Cerium-anomalies are not a result of igneous processes (Schreiber et al., 1980), but reflect terrestrial alteration. They are often present in achondrites recovered from Antarctica (Floss and Crozaz, 1991; Schreiber et al., 1980). In such cold desert environments, trivalent LREE can be leached from samples by terrestrial weathering, while tetravalent Ce may be retained in the host mineral (Floss and Crozaz, 1991). Winona, however, was not recovered from a cold desert location but was discovered in Arizona in 1928. To account for the discrepancy, it was suggested that Winona may have been transported south from a cold desert region (Greenwood et al., 2012), and our new data for this piece of Winona support this inference. High concentrations of fluid-mobile elements such as Ba also agree with the conclusion that this piece of Winona is extensively weathered. Due to the extent of weathering and uncertainty about the original trace-element composition, we exclude chemical data for our Winona sample from the following discussion.

#### **4.3 *Winonaite Precursor composition***

The winonaite-IAB parent body has previously been described as ‘chondritic’ on the basis of its approximately chondritic bulk element compositions and mineralogy (Benedix et al., 1998; Wasson et al., 1980). Other evidence for a chondritic precursor includes relict chondrules in Pontlyfni, and enstatite-like trapped noble gases in winonaites and IAB irons (Benedix et al., 1998). The chondritic nature of the precursor is also supported by our new modal analyses (Table 2; Figure 1) and the presence of chondrules and relict chondrules in NWA 1463 (Electronic Annex, Fig. S1). The interpretation of NWA 1463 as a primitive winonaite, however, was questioned when it was paired with NWA 725 (Irving and Rumble, 2006), which was originally classified as an acapulcoite. Recent O isotope studies have

shown, however, that both NWA 1463 and 725 plot with the winonaites (Greenwood et al., 2012). Although oxygen isotopes have confirmed this link, there are still enough differences that any interpretation of NWA 1463 should keep this uncertainty in mind.

Oxygen isotope data for the winonaites have a mean  $\Delta^{17}\text{O}$  of  $-0.51\text{‰}$ , with  $\delta^{18}\text{O}$  values ranging from  $2.84$  to  $7.21\text{‰}$  (Greenwood et al., 2012). On an oxygen three-isotope plot these data define a mass fractionation line with a slope of  $-0.53 \pm 0.01$ , implying planetary processing and homogenisation occurred on the winonaite parent body (Greenwood et al., 2012). Furthermore, the negative  $\Delta^{17}\text{O}$  suggests a link to the carbonaceous chondrites (Wasson and Kallemeyn, 2002). However, the winonaites have O isotope compositions unlike any known carbonaceous chondrite class (Clayton and Mayeda, 1996; Greenwood et al., 2012).

Major- and trace-element data for unweathered winonaites where silicate partial melts have not been removed (i.e., Fortuna, QUE 94535 and HaH 193, Pontlyfni and NWA 1463) can help elucidate the nature of the precursor material. Molar ratios of major-elements can be used to discriminate between different chondrite classes. Once Winona and Tierra Blanca are excluded (affected by weathering and silicate melting processes, respectively), the average bulk winonaite data indicate a general affinity to both ordinary and enstatite chondrites. The compositions of individual samples, however, also show some similarities to various carbonaceous chondrite groups (Fig. 4a-c).

In the following, trace-element data for the winonaites are compared to ordinary (H, L, LL), enstatite (EH, EL) and carbonaceous chondrites (CI, CM, CO, CV, CR). When normalized to Mg and ordered by volatility (50 % condensation temperature, 50 %  $T_c$ ; Fig. 7a), refractory elements reveal less variability than moderately volatile and highly volatile elements. Many elements (e.g., Cr, P, Ga, Na, K) show a slight depletion in the winonaites HaH 193, Fortuna and QUE 94535 relative to CI (Fig. 7a). In general, refractory elements (50 %  $T_c > 1301\text{ K}$ ) show similarities to ordinary chondrites (Fig. 7b). However, the winonaites

are slightly enriched in the moderately volatile elements (50 %  $T_c$  between ~ 660 and 1300 K) relative to the ordinary chondrites.

Reduced enstatite chondrite-like material is a possible precursor for the winonaites, and this association is also suggested by trapped noble gases (Benedix et al., 1998). Indeed, bulk samples of winonaites also show many elemental similarities to the enstatite chondrites (Figs. 4 a-c and 7c), in particular the nearly identical abundances of highly refractory elements. However, the winonaites are slightly depleted in the volatile elements compared to enstatite chondrites. In addition, the high carbon contents of the winonaites (up to 0.8 wt % in Pontlyfni; Grady and Pillinger, 1986) and IAB irons (0.4 – 1.0 wt %; Buchwald, 1975; Wasson and Kallemeyn, 2002) may preclude the enstatite chondrites, which typically have only 0.15 - 0.7 wt % C (Grady et al., 1986), as suitable precursor material.

For HaH 193, Fortuna and QUE 94535 the depletion of the volatile elements relative to CI is particularly pronounced (Fig. 7a), indicative of a precursor more volatile-depleted than CIs and possibly similar to CV, CM, CO or CR chondrites. However, the refractory element trend is diagnostic in CV and CO chondrites, and points to the abundance of calcium-aluminium-rich inclusions (CAIs) in these groups. In detail, the winonaites are depleted in refractory elements, and hence CAIs, relative to CV and CO chondrites, and these groups, therefore, do not represent the precursor materials for the winonaite parent body. The CM chondrites provide the closest match to the winonaites for a range of refractory and moderately volatile elements but they are slightly depleted in highly volatile elements relative to this group (Fig. 7d) and a perfect fit is thus not obtained. Data for the extinct Pd-Ag decay system also indicates that the winonaite-IAB parent body had a low, carbonaceous chondrite-like Pd/Ag ratio (Theis et al., 2013). In contrast to the generally more volatile-depleted magmatic iron parent bodies, this implies that the winonaite-IAB parent body may have

initially formed at a greater radial distance from the sun (0.5 – 1.5 AU versus 1.5 – 2 AU, respectively; Bottke et al., 2006).

In summary, the winonaite precursor most likely had a carbonaceous chondrite-like trace-element composition, although it also shared some major and trace-element characteristics with both ordinary and enstatite chondrites. The winonaite parent body was slightly volatile-depleted relative to CI, with a trace-element signature most akin to CM chondrites. However, the CM chondrites do not represent the precursor material for the winonaite parent body, and oxygen isotopes suggest that the winonaite precursor is not currently sampled in our collections (Clayton and Mayeda, 1996).

#### **4.4 *The Winonaite-IAB parent body in comparison to other primitive achondrites***

Compared to the primitive achondrite groups of brachinites, acapulcoites and lodranites, the winonaites retain textures and chemical compositions that imply more limited partial melting on their parent body. Acapulcoites and lodranites are thought to originate from the same parent body as residues of partial melting. The acapulcoites represent regions of a chondritic precursor which were heated to between the Fe, Ni-FeS cotectic and the silicate melting point (McCoy et al., 1996). In this respect, they are similar to the winonaites studied here, which also show limited chemical and textural evidence for silicate partial melting processes.

The lodranites are residues of both Fe, Ni-FeS and silicate partial melting (McCoy et al., 1997b). The same conclusion stands for the brachinites, although they originate from a distinct parent body (e.g., Day et al., 2012; Gardner-Vandy et al., 2013). Of the winonaites studied here, only Tierra Blanca shows chemical evidence for silicate melt extraction, making it comparable to the lodranites and brachinites. Some IAB silicate inclusions, for example Udei Station, also include lithologies formed as residues of silicate partial melting, whilst

other silicate inclusions, for example in Caddo County, are interpreted to represent trapped basaltic melts (Benedix et al., 2000; Ruzicka and Hutson, 2010; Takeda et al., 2000).

## 5. Temporal and Thermodynamic history of the winonaite body

Three models have been proposed to explain the geochemical evolution of the winonaite-IAB parent asteroid: 1) localized metallic impact melt pools (Wasson and Kallemeyn, 2002; Wasson et al., 1980); 2) incomplete differentiation (Takeda et al., 1994); and 3) incomplete differentiation followed by catastrophic impact break-up and reassembly (Benedix et al., 2000).

Textural evidence, such as the angular silicate-dominated regions surrounded by metal and troilite in Pontlyfni (Fig. 2, Supplementary Appendix Figure S7) or the juxtaposition of coarse and fine-grained regions in Winona (Benedix et al., 1998), implies that at least one impact and scrambling event is required to explain the brecciated nature of these meteorites (Benedix et al., 2000; Wasson and Kallemeyn, 2002). This rules out incomplete differentiation as the sole driver of the parent body evolution. It is also unlikely that localized impact melt pools alone can account for the evolution of the winonaite-IAB parent body because of the range of silicate metamorphism and melting observed in the inclusions of the IAB irons.

A number of textural and compositional features indicate that silicate partial melting and metamorphism must have occurred on the parent body prior to the event that generated mixing of metal and silicate phases. This includes, 1) a gabbroic texture in Caddo County (Benedix et al., 2000; Takeda et al., 2000); 2) the removal of a basaltic component from Udei Station silicates (Benedix et al. 2000; Ruzicka and Hutson, 2010); and 3) the presence of metallic veins cross-cutting metamorphosed silicate material. This evidence is inconsistent with an impact, which would both scramble the body and generate essentially simultaneous

melting (Davison et al., 2012). Furthermore, the very narrow temperature range to which the winonaites were heated (~1220 - 1370 K) is difficult to reconcile with impact melting. Additionally, Davison et al. (2013) have compared the sequence of thermal events on the winonaite-IAB parent body with their model for collisional evolution of solar system bodies. They find that only 0.1 % of bodies modelled (out of a total of  $10^5$ ) had impact-only histories which matched the heating events proposed for the winonaite parent body. This indicates that it is extremely difficult to account for the thermal history of the winonaite parent with an impact-only evolution.

Our new data are in good accord with a model of incomplete differentiation followed by catastrophic impact-induced break-up and reassembly, and they can furthermore be combined with results from previous studies to reconstruct the history of the winonaite-IAB parent body. The earliest recorded thermal episode on this body is the metal-silicate segregation that affected IAB metal phases at  $3.6^{+2.3/-2.0}$  Ma after CAI formation ( $^{182}\text{Hf}$ - $^{182}\text{W}$ , Schulz et al., 2009; recalculated relative to latest CAI value, Kruijer et al., 2014). Comparison to the thermal model of Qin et al. (2008) suggests that an asteroid undergoing metal-silicate segregation at  $3.6^{+2.3/-2.0}$  Ma must have accreted at ~ 1.8 Ma. The melting was thereby sufficiently early to be a parent body-wide response to internal heating from the decay of short-lived  $^{26}\text{Al}$  and  $^{60}\text{Fe}$ . Textural evidence for the migration of molten metal and sulfide is recorded by the winonaites, in particular Pontlyfni and Fortuna, and can be viewed as a resulting from large-scale heating to at least the Fe, Ni - FeS cotectic (1223 K), followed by incipient core formation. However, the survival of a chondritic mineralogy, i.e., the winonaites and some IAB silicate inclusions, indicates that core-mantle differentiation on the parent body was incomplete.

Silicate inclusions in IAB iron meteorites have a variety of compositions, from metamorphosed chondritic lithologies to the products and residues of between about 3 and 10

% silicate partial melting (Fig. 6), implying a peak temperature of ~1450 K (Benedix et al., 2000; Ruzicka and Hutson, 2010). Three IAB silicate inclusions analysed for  $^{182}\text{Hf}$ - $^{182}\text{W}$  were interpreted to correspond to silicate differentiation on the parent body at  $3.1^{+2.3}/_{-1.9}$  Ma after CAI formation, which is within uncertainty of the metal segregation event recorded by the IAB irons (Schulz et al., 2009; recalculated relative to latest CAI value, Kruijer et al., 2014). However, this differentiation event is not recorded by the winonaites, which show only limited trace-element evidence for partial melting of silicates (i.e., Fig. 4a), indicating they reached a peak temperature of < 1370 K. Taken together, these findings imply heterogeneous heat distribution within the parent body. In this scenario, the IAB irons and silicate lithologies that are indicative of higher temperatures originate from deeper within the parent body, whilst the winonaites with their lower peak temperatures originate in the outer layers.

On the one hand, Fe, Ni-metal and sulphide textures in the winonaites, and the abundance of IAB irons, suggest that the parent body began to differentiate and form at least one metallic body. Formation of multiple metal pools is inferred from trace-element data that distinguish between numerous 'sub-groups' of IAB irons (Wasson and Kallemeyn, 2002; Worsham et al., 2016). On the other hand, the presence of relict chondrules, the chondritic mineralogy of winonaites, and the lack of major- and trace-element evidence for silicate melting suggest that the differentiation process did not complete. There are two possible explanations for this. The first is that the parent body was too small or did not accrete early enough to achieve complete differentiation. Estimates for the winonaite parent body radius range from ~30 to 100 km (Benedix et al., 2014; Benedix et al., 2005; Herpfer et al., 1994), and accretion is inferred to take place at ~1.8 Ma after CAIs. A comparison with the thermal models of Lichtenberg et al. (2016) indicates that an asteroid with such characteristics is unlikely to reach the temperatures required to fully differentiate into a core and mantle by internal heating. However, such a body would reach the Fe, Ni-FeS cotectic temperature, providing an explanation for the textural evidence of metallic melts in the winonaites, and

also the lack of geochemical evidence for silicate melting. Depending on the exact size of the body, the interior may remain at temperatures above the Fe, Ni-FeS cotectic for several Ma (Lichtenberg et al., 2016), thereby accounting for the extensive metamorphism of the winonaites. Additionally, this may provide a mechanism for generating the winonaite O isotope mass fractionation line ( $-0.53 \pm 0.01$ ; Greenwood et al., 2012) via high temperature thermal diffusion of oxygen isotopes (Bindeman et al., 2013)

A comparison to the acapulcoite-lodranite parent asteroid implies a second process took place to halt differentiation on the winonaite parent body. Estimates for the radius of the acapulcoite-lodranite parent body are similar to the inferred size of the winonaite parent (25 – 100 km; Golabek et al., 2014; Touboul et al., 2009). The winonaite-IAB parent body is furthermore inferred to have accreted slightly earlier than the acapulcoite-lodranite parent (Schulz et al., 2010). Hence, although the winonaite-IAB parent body may never have fully completed differentiation, it should have experienced heating and melting to an extent that is comparable to or even larger than that of the acapulcoite-lodranite parent asteroid. This and the brecciated nature of the winonaites strongly suggests an additional process occurred on the winonaite parent body and arrested core formation.

The heterogeneous and juxtaposed lithologies of the winonaites and IAB silicate inclusions have led several authors to conclude that the winonaite-IAB parent body was shaped by catastrophic impact disruption and subsequent gravitational re-assembly of the debris (Benedix et al., 2005; Benedix et al., 2000; Ruzicka and Hutson, 2010; Theis et al., 2013; Vogel and Renne, 2008). This is in agreement with textural evidence from the winonaites studied here, which suggests that scrambling of the different lithologies occurred when Fe, Ni metal and sulfide were still molten, whilst some silicate-rich areas were unaffected by melting processes (i.e., Fig. 2b). Impact disruption and re-assembly would have effectively terminated core formation on the winonaite parent body. Additionally, impact

disruption would lead to increased cooling rates for the parent body (Ciesla et al., 2013), and this would further impede the differentiation process. Palladium-silver ages for IAB iron meteorites indicate that the last thermal event on the parent body to reach temperatures high enough to melt metal occurred ~10 -14 Ma after CAI (Theis et al., 2013). This timescale is in accord with the similar  $^{182}\text{Hf}$ - $^{182}\text{W}$  ages of IAB irons, which record a thermal event that is interpreted to reflect the catastrophic impact disruption of the winonaite-IAB parent body (Markowski et al., 2006; Schulz et al., 2009; Schulz et al., 2012).

## 6. Conclusions

The winonaites are primitive achondrites with textures that imply heating to at least the Fe, Ni-FeS cotectic. Of the samples analysed here, only one (Tierra Blanca) shows geochemical evidence for silicate melting processes. All other winonaites studied have chondritic major-element ratios and flat CI normalised rare-earth element patterns. This suggests that the majority of the winonaites were heated only to between ~1220 and 1370 K, most likely as a consequence of internal heating from the decay of short-lived radionuclides. However, the winonaite-IAB parent body did not fully differentiate into a metallic core and silicate mantle. The brecciated nature of the winonaites suggests that the parent body was disrupted by an impact whilst close to its peak temperature, at between 10 and 14 Ma after CAI. This impact halted differentiation and enabled the preservation of winonaites with little or no evidence of silicate partial melting. Despite major-element similarities to both the ordinary chondrite and enstatite chondrite groups, an expanded set of trace-element data indicates that the winonaite parent body had a carbonaceous chondrite-like composition. The parent body was volatile-depleted relative to CIs, and shares trace-element characteristics with CM chondrites. However, CM chondrites ultimately do not represent the winonaite-IAB precursor material, which is not sampled in current meteorite collections.

*Acknowledgements* This work was financially supported by the Leverhulme Trust through grant F/00 696/R. Many thanks to Anton Kearsley at the Natural History Museum in London for assistance with SEM analyses, and Caroline Smith and Deborah Cassey at the Natural History Museum for providing additional samples for this study. We also thank Kathryn Gardner-Vandy and Ed Scott for their thoughtful and instructive reviews, and Anders Meibom for editorial handling of this manuscript.

ACCEPTED MANUSCRIPT

## Tables

**Table 1.** Winonaite samples analysed for this study and material sources.

| Sample                      | Polished thin section      | Source of bulk material for major- and trace-element analysis |
|-----------------------------|----------------------------|---|
| Fortuna                     | M 57                       | Natural History Museum, Berlin                                |
| Hammadah al Hamra 193       | PL 96276                   | University of Münster   |
| Mount Morris (Wisc.)        | UH 157 <sup>‡</sup>        | N/A   |
| Northwest Africa 1463       | 3B                         | Smithsonian Institution                                       |
| Pontlyfni                   | BM 1975, M6.1 <sup>Δ</sup> | BM 1975, M6; Natural History Museum, London                   |
|                             | BM 1975, M6.2 <sup>Δ</sup> |   |
|                             | BM 1975, M6.3 <sup>Δ</sup> |   |
| Queen Alexander Range 94535 | ,16                        | Meteorite Working Group, NASA                                 |
| Tierra Blanca               | N/A                        | BM 1982, M12; Natural History Museum, London                  |
| Winona                      | AMNH 4158-1*               | Smithsonian Institution                                       |
|                             | AMNH 3768*                 |   |
|                             | USNM 854 <sup>+</sup>      |   |
|                             | UH 195 <sup>‡</sup>        |   |
|                             | UH 133 <sup>‡</sup>        |   |
|                             | BM 1930,974 <sup>Δ</sup>   |   |

Thin section sources: \*American Museum of Natural History; <sup>+</sup>Smithsonian Institution; <sup>‡</sup>University of Hawaii; <sup>Δ</sup>Natural History Museum, London; N/A, no analysis made.

**Table 2.** Modal mineralogy for winonaite samples in volume %.

| Sample                                 | Fortuna | HaH<br>193  | Mt<br>Morris | NWA<br>1463 | Pontlyfni |      |      | QUE<br>94535 | Winona       |                |                |           |           |             |
|--|---------|-------------|--------------|-------------|-----------|------|------|--------------|--------------|----------------|----------------|-----------|-----------|-------------|
|  | M57     | PL<br>96276 | UH<br>157    | 3B          | M6.1      | M6.2 | M6.3 | ,16          | AMNH<br>3768 | AMNH<br>4158-1 | BM<br>1930,974 | UH<br>133 | UH<br>195 | USNM<br>854 |
| PTS Identifier                         |         |             |              |             |           |      |      |              |              |                |                |           |           |             |
| PTS area, mm <sup>2</sup><br>(approx.) | 102     | 87          | 133          | 102         | 46        | 34   | 63   | 38           | 81           | 213            | 16             | 104       | 137       | 306         |
| Electronic Annex<br>Figure             | S1      | S2          | S3           | S4          | S5        | S6   | S7   | S8           | S9           | S10            | S11            | S12       | S13       | S14         |
| Metal <sup>a</sup>                     | 7.67    | 26.6        | 38.2         | 16.0        | 9.8       | 13.5 | 15.3 | 9.76         | 48.6         | 18.4           | 41.6           | 16.9      | 33.0      | 13.9        |
| Troilite                               | 7.1     | 3.1         | 5.2          | 8.8         | 19.7      | 20.7 | 22.7 | 6.6          | 2.9          | 4.1            | 11.5           | 3.5       | 5.4       | 7.1         |
| Olivine                                | 24.7    | 17.0        | 10.0         | 10.4        | 16.6      | 12.8 | 11.7 | 24.0         | 10.5         | 24.3           | 0.14           | 21.5      | 21.1      | 22.9        |
| Low-Ca Pyroxene                        | 39.1    | 36.1        | 30.1         | 48.8        | 34.6      | 35.5 | 30.0 | 41.3         | 21.2         | 32.8           | n.d.           | 41.6      | 30.4      | 36.1        |
| Plagioclase                            | 16.3    | 13.6        | 15.5         | 6.4         | 14.6      | 12.3 | 15.6 | 14.8         | 15.7         | 19.7           | 37.0           | 15.9      | 9.4       | 19.4        |
| Calcic Pyroxene                        | 4.6     | 1.9         | 0.2          | 8.7         | 3.3       | 4.1  | 1.9  | 2.9          | 0.5          | 0.3            | 9.7            | 0.1       | n.d.      | 0.2         |
| Phosphate                              | 0.3     | 0.1         | n.d.         | 0.4         | n.d.      | n.d. | n.d. | n.d.         | 0.7          | 0.4            | n.d.           | 0.3       | 0.4       | 0.4         |
| Chromite                               | 0.2     | tr          | tr           | 0.3         | n.d.      | n.d. | n.d. | tr           | tr           | 0.1            | n.d.           | tr        | 0.1       | 0.1         |
| Schreibersite                          | n.d.    | 0.2         | 0.7          | 0.1         | 1.3       | 0.6  | 0.7  | 0.7          | n.d.         | tr             | n.d.           | 0.1       | 0.1       | n.d.        |
| Daubreeelite                           | n.d.    | n.d.        | n.d.         | n.d.        | 0.2       | 0.2  | 2.3  | tr           | n.d.         | n.d.           | n.d.           | n.d.      | n.d.      | n.d.        |
| Alabandite                             | n.d.    | n.d.        | n.d.         | n.d.        | n.d.      | 0.3  | n.d. | tr           | n.d.         | n.d.           | n.d.           | n.d.      | n.d.      | n.d.        |
| Amphibole                              | n.d.    | 1.4         | n.d.         | n.d.        | n.d.      | n.d. | n.d. | n.d.         | n.d.         | n.d.           | n.d.           | n.d.      | n.d.      | n.d.        |
| Total                                  | 100     | 100         | 100          | 100         | 100       | 100  | 100  | 100          | 100          | 100            | 100            | 100       | 100       | 100         |

The standard deviation of each individual measurement is better than 1.7 % in all cases. See text for description of mineral mode determination. <sup>a</sup>Mode for metal includes Fe-rich weathering products, produced from both metal and troilite. tr, less than 0.1 % detected; n.d., not detected in section. Montaged element X-ray maps are available in the Electronic Annex.

**Table 3.** Whole-rock ICP-AES major element data for the winonaites. Except where stated, all values are given as wt. %.

|                                | Fortuna | HaH 193 | NWA<br>1463 | Pontlyfni | QUE<br>94535 | Terra<br>Blanca | Winona |       |
|--------------------------------|---------|---------|-------------|-----------|--------------|-----------------|--------|-------|
| SiO <sub>2</sub>               | 40.2    | 38.2    | 35.7        | 32.1      | 46.1         | 32.4            | 15.7   |       |
| TiO <sub>2</sub>               | 0.11    | 0.09    | 0.10        | 0.04      | 0.07         | 0.07            | 0.09   |       |
| Al <sub>2</sub> O <sub>3</sub> | 2.46    | 2.41    | 1.87        | 1.94      | 2.73         | 0.99            | 2.70   |       |
| FeO(t)*                        | 24.9    | 23.3    | 35.1        | 34.7      | 14.0         | 30.0            | 47.8   |       |
| MnO                            | 0.33    | 0.19    | 0.31        | 0.27      | 0.22         | 0.51            | 0.08   |       |
| MgO                            | 25.9    | 24.4    | 21.0        | 22.3      | 29.3         | 22.5            | 3.57   |       |
| CaO                            | 1.64    | 1.91    | 1.39        | 1.63      | 1.44         | 0.62            | 1.67   |       |
| Na <sub>2</sub> O              | 1.1     | 0.98    | 0.89        | 0.94      | 1.1          | 0.37            | 1.16   |       |
| K <sub>2</sub> O               | 0.07    | 0.06    | 0.12        | 0.09      | 0.04         | 0.04            | 0.12   |       |
| P <sub>2</sub> O <sub>5</sub>  | 0.20    | 0.26    | 0.23        | 0.41      | 0.29         | 0.15            | 0.18   |       |
| Cr                             | ppm     | 2907    | 901         | 2866      | 2725         | 885             | 2732   | 1322  |
| Ni                             | ppm     | 11090   | 13470       | 19940     | 23020        | 12730           | 19890  | 19060 |
| Total                          |         | 98.35   | 93.15       | 98.98     | 97.02        | 96.7            | 89.91  | 75.07 |

The external reproducibility of each measurement by ICP-AES is better than 10 % (RSD), except Ni (17 %) and FeO(t) (24 %). See discussion in text for further details. \*All Fe (including Fe, Ni metal) is expressed as FeO(t).

**Table 4.** Whole-rock ICP-MS trace element data for the winonaites. All values are given as ppm.

|    | Fortuna | HaH 193 | QUE<br>94535 | Winona |
|----|---------|---------|--------------|--------|
| Li | 1.84    | 2.02    | 1.61         |        |
| Sc | 7.13    | 9.31    | 9.36         | 6.3    |
| V  | 42.8    | 21.1    | 30.1         | 31.1   |
| Co | 622     | 728     | 367          | 1590   |
| Cu | 44.7    | 26.6    | 69           |        |
| Zn | 234     | 111     | 42.5         |        |
| Ga | 16.3    | 6.78    | 8.46         | 14.7   |
| Rb | 0.89    | 0.48    | 0.75         | 2.8    |
| Sr | 9.46    | 16.5    | 14.6         | 19.3   |
| Y  | 1.42    | 1.81    | 2.23         | 3.7    |
| Zr | 2.9     | 4.48    | 5.17         | 16     |
| Nb | 0.07    | 0.2     | 0.13         | 0.6    |
| Rh | 0.22    | 0.18    | 0.26         |        |
| Pd | 0.06    | 0.07    | 0.19         |        |
| Sn | 0.73    | 0.93    | 1.17         |        |
| Sb | 0.06    | 0.08    | 0.10         |        |
| Cs | 0.02    | 0.02    | 0.05         |        |
| Ba | 3.62    | 2.6     | 4.29         | 30.9   |
| La | 0.57    | 0.24    | 0.43         | 4.80   |
| Ce | 1.75    | 0.59    | 1.05         | 26.2   |
| Pr | 0.15    | 0.09    | 0.16         | 0.70   |
| Nd | 0.66    | 0.43    | 0.78         | 2.86   |
| Sm | 0.20    | 0.18    | 0.29         | 0.62   |
| Eu | 0.08    | 0.07    | 0.11         | 0.16   |
| Gd | 0.25    | 0.28    | 0.39         | 0.79   |
| Tb | 0.05    | 0.05    | 0.07         | 0.11   |
| Dy | 0.29    | 0.34    | 0.47         | 0.66   |
| Ho | 0.06    | 0.08    | 0.10         |        |
| Er | 0.19    | 0.23    | 0.31         | 0.35   |
| Tm | 0.03    | 0.03    | 0.05         | 0.05   |
| Yb | 0.20    | 0.23    | 0.36         | 0.28   |
| Lu | 0.04    | 0.04    | 0.05         | 0.04   |
| Hf | 0.24    | 0.27    | 0.27         |        |
| Ir | 0.67    | 0.61    | 1.22         |        |
| Pt | 1.36    | 1.13    | 1.91         |        |
| Au | 0.24    | 0.21    | 0.17         |        |
| Pb | 1.84    | 0.85    | 1.47         |        |
| Th | 0.11    | 0.12    | 0.11         |        |

The external reproducibility of each measurement by ICP-MS is better than 5 % (2 RSD).

**Figure captions**

**Figure 1.** Modal abundance (volume %) of major mineral phases present in the winonaites.

Mineral modes were calculated from montaged SEM X-ray maps. For further details see text.

\*Metal includes Fe-rich weathering product from metal and troilite. Accessory phases including phosphate, chromite, schreibersite, daubreélite, alabandite and amphibole are omitted here. Abundances for these and all mineral phases are given in Table 2.

**Figure 2.** a. Montaged and combined element X-ray maps (Ca-Si-Mg + S-Fe-Cr) for Winona (UH 133). UH 133 shows both veins and blebs of metal. Troilite is only present as blebs in this view. Silicates are generally equigranular. Pl., plagioclase; Ol., olivine; Px., low-Ca pyroxene; Ca-Px., calcic pyroxene; Ap., apatite; Metal, metal plus weathering product; Tr., troilite; Chr., chromite; Sch., schreibersite. b. Backscattered electron (BSE) map of Pontlyfni (M 6.2), showing the textures of metal (M), troilite (Tr) and bulk silicates (S). Metal, troilite and silicates are heterogeneously distributed throughout the section. Metal and troilite are present as large blebs and veins. The region marked '1' is a silicate-dominated area with an angular shape, surrounded by metal and troilite.

**Figure 3.** CI chondrite-normalised element abundances for HaH 193, Fortuna, QUE 94535 and Winona. Winona shows significant enrichment in Ba, La, and Ce, most likely due

extensive weathering. The other three meteorites do not have these enrichments and their patterns are nearly identical. Uncertainties are within the size of the symbol, unless shown.

Elements are ordered by increasing atomic number. Values for CI are taken from Anders and Grevesse (1989).

**Figure 4.** (a) Molar Mg/Si vs. Al/Si. Samples that represent partial melts have high Al/Si values (i.e., howardites and eucrites), while melt residues have high Mg/Si (i.e., lodranites and diogenites). The majority of winonaites plot with the chondrites, which did not experience melting. Tierra Blanca (TB) may represent a melt residue, while Winona (this study; W) plots as a melt product. (b) Molar Ca/Si vs. Al/Si and (c) molar Ti/Si vs. Al/Si. Note the Al/Si axis has been re-scaled to show more detail of the chondrites. As a result, Winona is not shown on (b) or (c) The winonaite average (excluding Winona and Tierra Blanca) plots between ordinary and enstatite chondrite. In most cases, individual winonaites plot with the ordinary and enstatite chondrites, whilst some samples overlap with CR and CI chondrites. Winonaite literature data from Graham et al. (1977), King et al. (1981), and Mason and Jarosewich (1967). IAB inclusion data from Jarosewich (1967), Kracher (1974), and Wlotzka and Jarosewich (1977). Acapulcoite and Lodranite data from Mittlefehldt et al. (1998). Howardite, eucrite and diogenite data from Dodd (1981) and Jarosewich (1990). All chondrite data are taken from Jarosewich (1990), Wiik (1956), and Yanai & Kojima (1995).

**Figure 5.** Chondrite-normalised bulk REE abundances for the winonaites. Filled black symbols are results from this study. Winona exhibits a very different pattern for LREE, with La, Ce, Pr, and Nd all significantly enriched. This is primarily due to alteration. All other samples from this study have relatively flat REE patterns. Uncertainties are within the size of the symbol. Additional winonaite data (marked with asterisks) is also plotted for comparison. Data are from Prinz et al. (1980) and Floss et al. (2007, 2008). Values for CI taken from Anders and Grevesse (1989).

**Figure 6.** Element abundances for the winonaites normalised to CI (Anders and Grevesse, 1989). Also included are (a) modelled residue compositions and (b) modelled melt compositions after varying degrees of melting (F) for a parent body with a starting composition of CM chondrite (see section 4.3 for discussion of precursor composition). Data for two IAB silicate inclusions from Udei Station are included. These plot as residues (3B) or melts (1B) (Ruzicka and Hutson, 2010), consistent with mineralogical evidence (Benedix et al., 2000). Uncertainties are within the size of the symbol, unless shown. Data for CM chondrites from Wasson and Kallemeyn (1988). Melting model and partition coefficients are taken from Ruzicka & Hutson (2010). Elements are ordered by increasing atomic number.

**Figure 7.** Chondrite- and Mg-normalised plots of winonaite lithophile elements, whereby volatility increases to the right. Data are normalised to different chondrite classes in order to assess the closest match for the winonaite precursor. The average of QUE 94535, HAH 193 and Fortuna is also shown. Overall, the refractory elements behave similarly and are close to CI in abundance. Variations are most discernible for elements more volatile than Nb. The winonaites are volatile-depleted relative to CI (a) but slightly more volatile-rich than H chondrites (b), which otherwise provide a good fit to the data. (c) The winonaites are volatile-depleted relative to EH. (d) CM chondrites provide the best fit to both refractory and moderately volatile elements but the winonaites are still slightly enriched in volatile elements relative to CM. Uncertainties (this dataset) are within the size of the point unless shown. Grey bands represent variations in the chondrite datasets. Data for chondrites are from Wasson & Kallemeyn (1988), except CI (Anders and Grevesse, 1989). Elements are ordered by decreasing 50 %  $T_c$  (Lodders, 2003).

## Figures

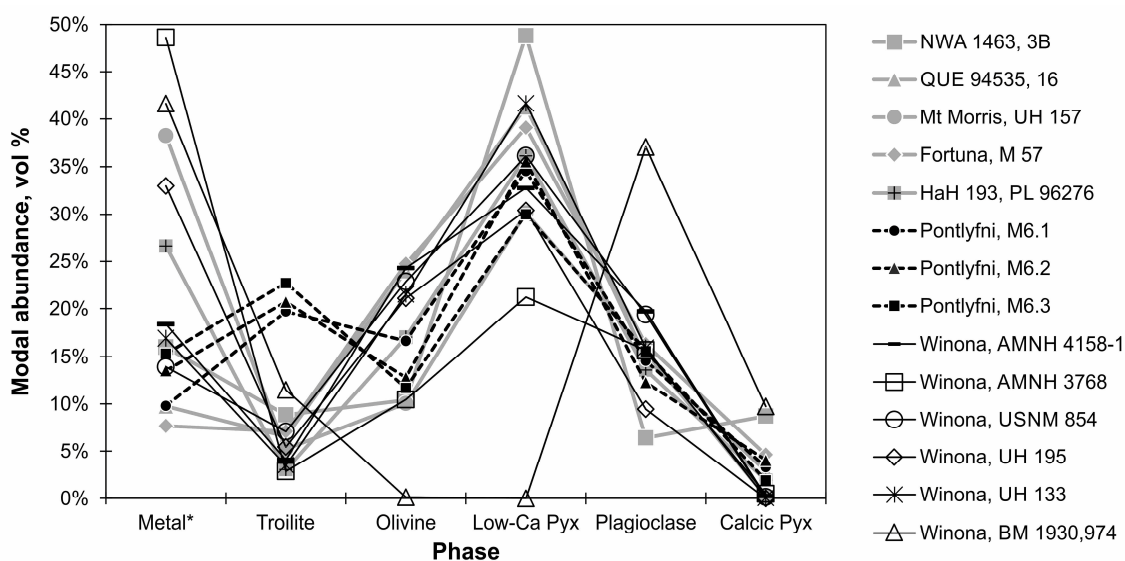


**Figure 1.** Modal abundance (volume %) of major mineral phases present in the winonaites.

Mineral modes were calculated from montaged SEM X-ray maps. For further details see text.

\*Metal includes Fe-rich weathering product from metal and troilite. Accessory phases including phosphate, chromite, schreibersite, daubreélite, alabandite and amphibole are omitted here. Abundances for these and all mineral phases are given in Table 2.

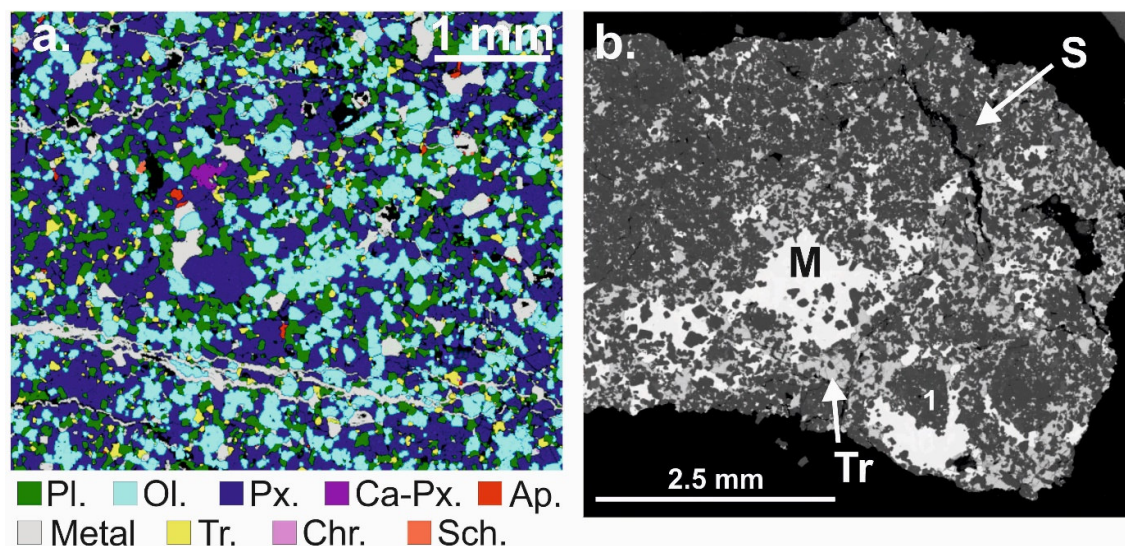


**Figure 2.** a. Montaged and combined element X-ray maps (Ca-Si-Mg + S-Fe-Cr) for Winona (UH 133). UH 133 shows both veins and blebs of metal. Troilite is only present as blebs in this view. Silicates are generally equigranular. Pl., plagioclase; Ol., olivine; Px., low-Ca pyroxene; Ca-Px., calcic pyroxene; Ap., apatite; Metal, metal plus weathering product; Tr., troilite; Chr., chromite; Sch., schreibersite. b. Backscattered electron (BSE) map of Pontlyfni (M 6.2), showing the textures of metal (M), troilite (Tr) and bulk silicates (S). Metal, troilite and silicates are heterogeneously distributed throughout the section. Metal and troilite are present as large blebs and veins. The region marked '1' is a silicate-dominated area with an angular shape, surrounded by metal and troilite.

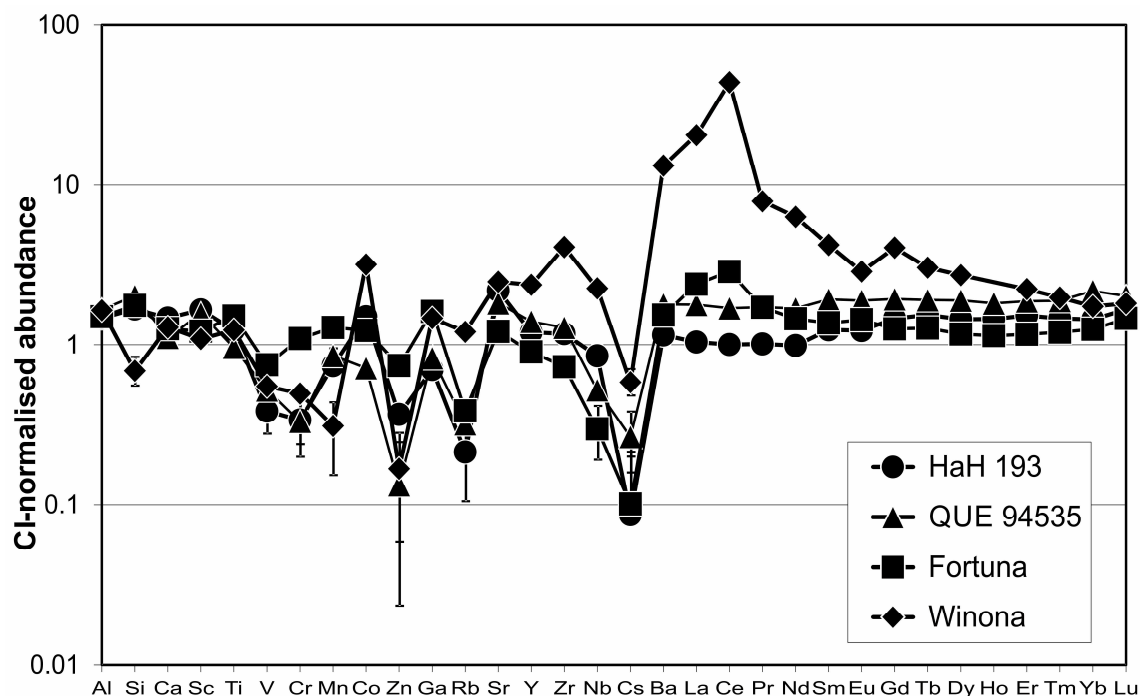


**Figure 3.** CI chondrite-normalised element abundances for HaH 193, Fortuna, QUE 94535 and Winona. Winona shows significant enrichment in Ba, La, and Ce, most likely due extensive weathering. The other three meteorites do not have these enrichments and their patterns are nearly identical. Uncertainties are within the size of the symbol, unless shown. Elements are ordered by increasing atomic number. Values for CI are taken from Anders and Grevesse (1989).

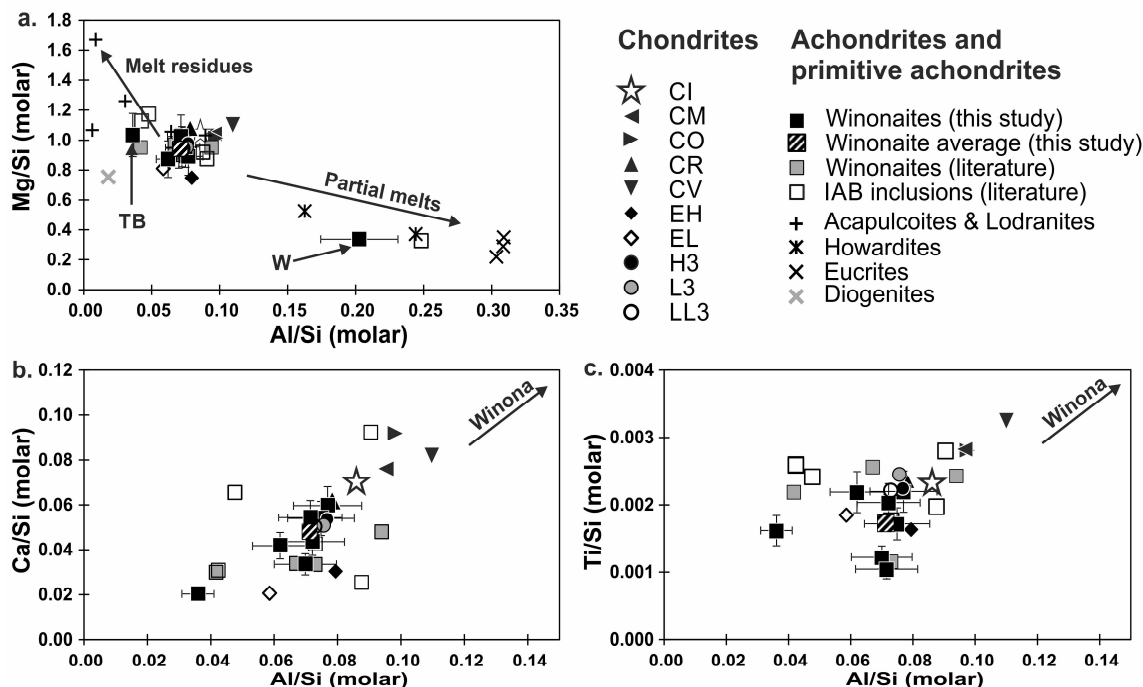


**Figure 4** (a) Molar Mg/Si vs. Al/Si. Samples that represent partial melts have high Al/Si values (i.e., howardites and eucrites), while melt residues have high Mg/Si (i.e., lodranites and diogenites). The majority of winonaites plot with the chondrites, which did not experience melting. Tierra Blanca (TB) may represent a melt residue, while Winona (this study; W) plots as a melt product. (b) Molar Ca/Si vs. Al/Si and (c) molar Ti/Si vs. Al/Si. Note the Al/Si axis has been re-scaled to show more detail of the chondrites. As a result, Winona is not shown on (b) or (c). The winonaite average (excluding Winona and Tierra Blanca) plots between ordinary and enstatite chondrite. In most cases, individual winonaites plot with the ordinary and enstatite chondrites, whilst some samples overlap with CR and CI chondrites. Winonaite literature data from Graham et al. (1977), King et al. (1981), and Mason and Jarosewich (1967). IAB inclusion data from Jarosewich (1967), Kracher (1974), and Wlotzka and Jarosewich (1977). Acapulcoite and Lodranite data from Mittlefehldt et al. (1998). Howardite, eucrite and diogenite data from Dodd (1981) and Jarosewich (1990). All chondrite data are taken from Jarosewich (1990), Wiik (1956), and Yanai & Kojima (1995).

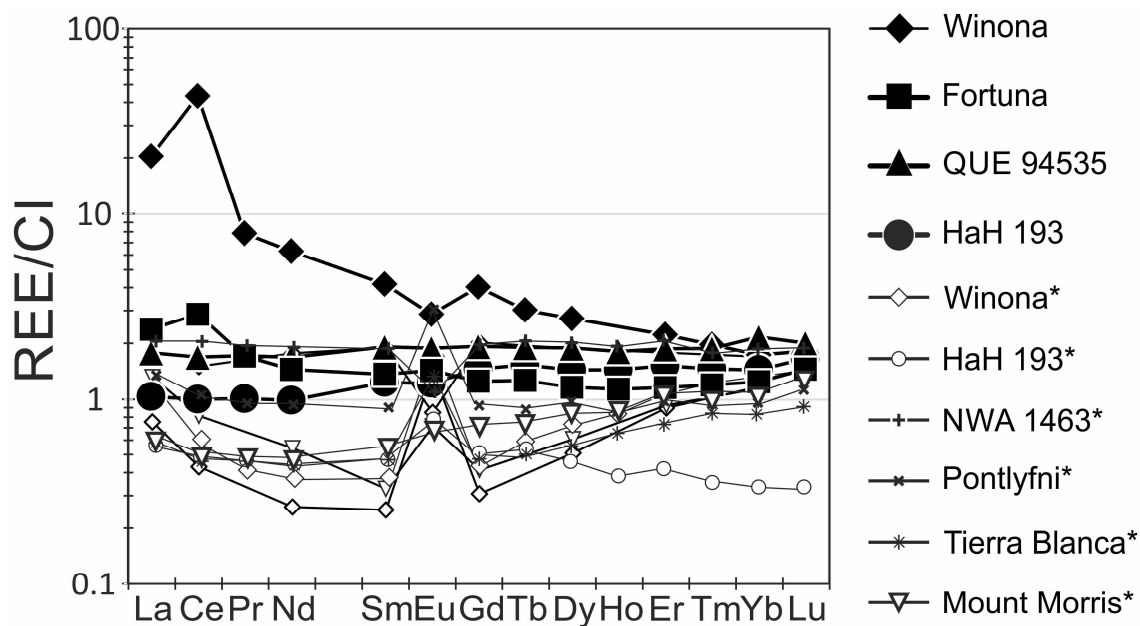


**Figure 5.** Chondrite-normalised bulk REE abundances for the winonaite. Filled black symbols are results from this study. Winona exhibits a very different pattern for LREE, with La, Ce, Pr, and Nd all significantly enriched. This is primarily due to alteration. All other samples from this study have relatively flat REE patterns. Uncertainties are within the size of the symbol. Additional winonaite data (marked with asterisks) is also plotted for comparison. Data are from Prinz et al. (1980) and Floss et al. (2007, 2008). Values for CI taken from Anders and Grevesse (1989).

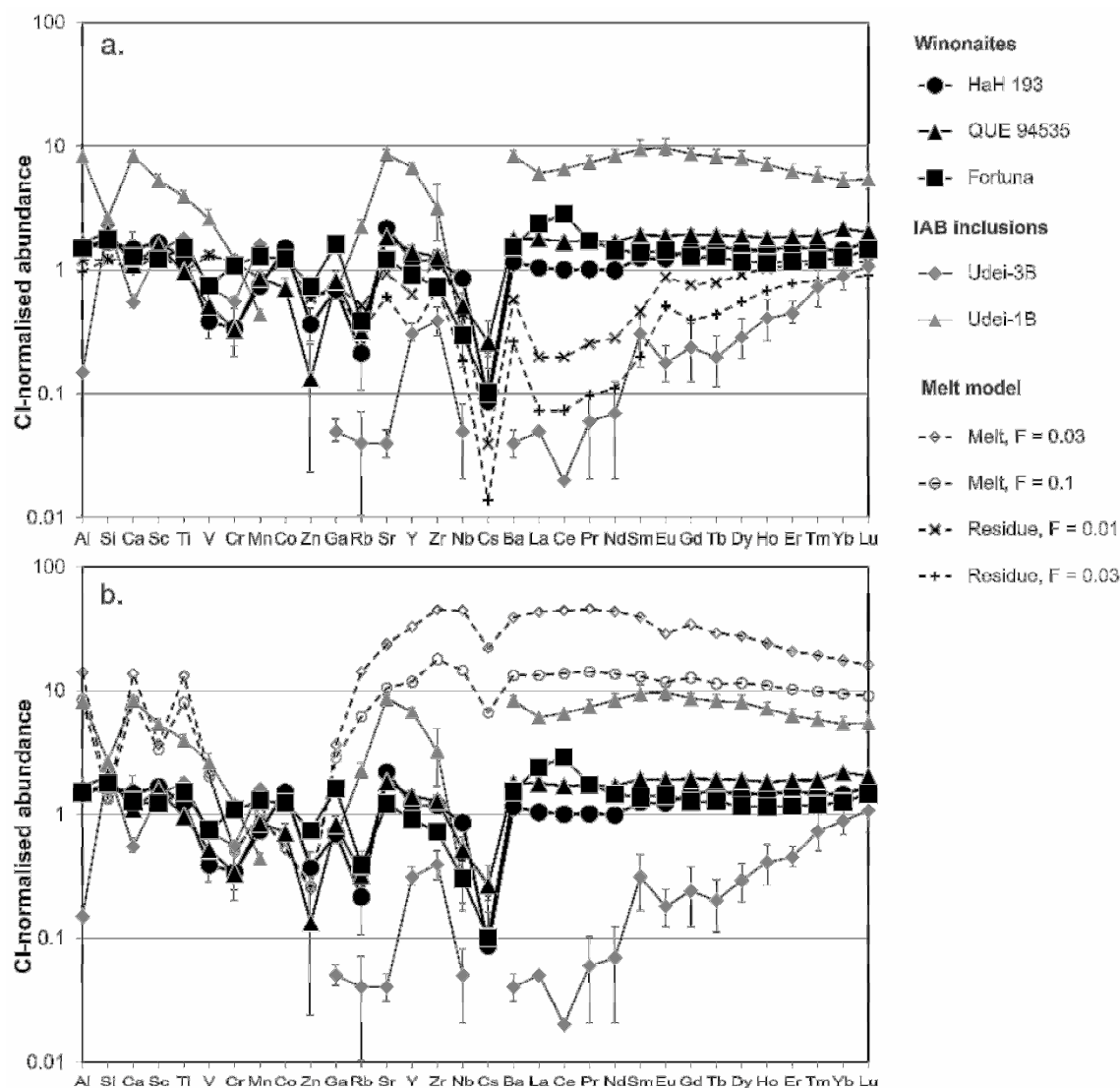


**Figure 6.** Element abundances for the winonaites normalised to CI (Anders and Grevesse, 1989). Also included are (a) modelled residue compositions and (b) modelled melt compositions after varying degrees of melting ( $F$ ) for a parent body with a starting composition of CM chondrite (see section 4.3 for discussion of precursor composition). Data for two IAB silicate inclusions from Udei Station are included. These plot as residues (3B) or melts (1B) (Ruzicka and Hutson, 2010), consistent with mineralogical evidence (Benedix et al., 2000). Uncertainties are within the size of the symbol, unless shown. Data for CM chondrites from Wasson and Kallemeyn (1988). Melting model and partition coefficients are taken from Ruzicka & Hutson (2010). Elements are ordered by increasing atomic number.

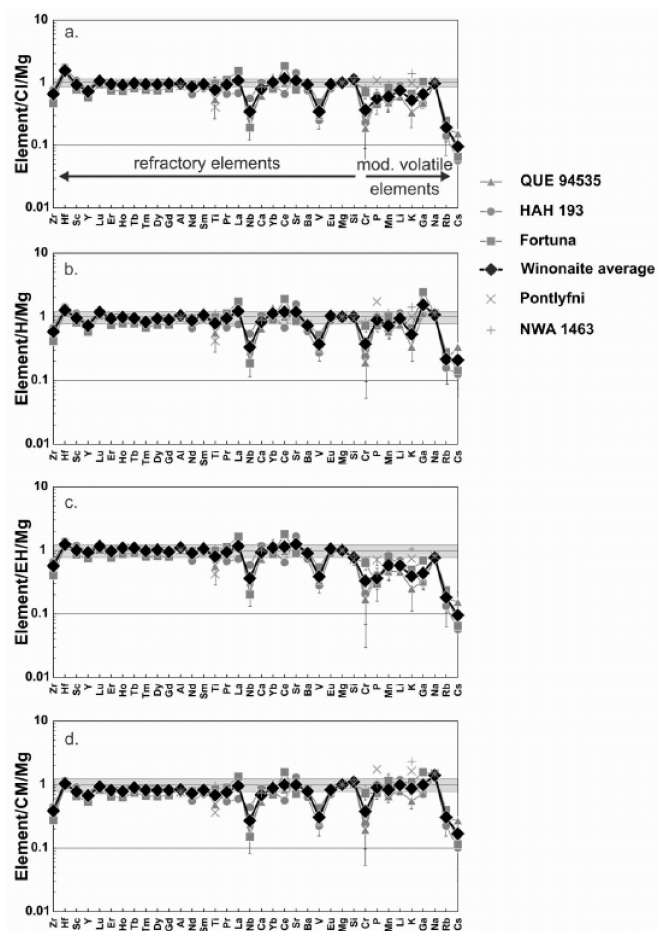


**Figure 7.** Chondrite- and Mg-normalised plots of winonaite lithophile elements, whereby volatility increases to the right. Data are normalised to different chondrite classes in order to assess the closest match for the winonaite precursor. The average of QUE 94535, HAH 193 and Fortuna is also shown. Overall, the refractory elements behave similarly and are close to CI in abundance. Variations are most discernible for elements more volatile than Nb. The winonaite is volatile-depleted relative to CI (a) but slightly more volatile-rich than H chondrites (b), which otherwise provide a good fit to the data. (c) The winonaite is volatile-depleted relative to EH. (d) CM chondrites provide the best fit to both refractory and moderately volatile elements but the winonaite is still slightly enriched in volatile elements relative to CM. Uncertainties are within the size of the symbol, unless shown. Grey bands represent variations in the chondrite datasets. Data for chondrites are from Wasson &

Kallemeyn (1988), except CI (Anders and Grevesse, 1989). Elements are ordered by decreasing 50 %  $T_c$  (Lodders, 2003).

ACCEPTED MANUSCRIPT

**References**

- Anders E. and Grevesse N. (1989) Abundances of the elements: Meteoritic and solar. *Geochim. Cosmochim. Acta* **53**, 197-214.
- Artemieva N. and Pierazzo E. (2009) The Canyon Diablo impact event: Projectile motion through the atmosphere. *Meteorit. Planet. Sci.* **44**, 25-42.
- Benedix G. K., McCoy T. J., Keil K., Bogard D. D. and Garrison D. H. (1998) A petrologic and isotopic study of winonaites: Evidence for early partial melting, brecciation, and metamorphism. *Geochim. Cosmochim. Acta* **62**, 2535-2553.
- Benedix G. K., McCoy T. J., Keil K. and Love S. G. (2000) A petrologic study of the IAB iron meteorites: Constraints on the formation of the IAB-Winonaite parent body. *Meteorit. Planet. Sci.* **35**, 1127-1141.
- Benedix G. K., McCoy T. J. and Lauretta D. S. (2003) Is NWA 1463 the most primitive winonaite? *Meteorit. Planet. Sci.* **30**, A70 (abstr.).
- Benedix G. K., Lauretta D. S. and McCoy T. J. (2005) Thermodynamic constraints on the formation conditions of winonaites and silicate-bearing IAB irons. *Geochim. Cosmochim. Acta* **69**, 5123-5131.
- Benedix G. K., Haack H. and McCoy T. J. (2014) 1.7 - Iron and Stony-Iron Meteorites, in: Holland, H.D., Turekian, K.K. (Eds.), *Treatise on Geochemistry (Second Edition)*. Elsevier, Oxford, pp. 267-285.
- Bild R. W. (1977) Silicate inclusions in group IAB irons and a relation to the anomalous stones Winona and Mt Morris (Wis). *Geochim. Cosmochim. Acta* **41**, 1439-1456.
- Bindeman I. N., Lundstrom C. C., Bopp C. and Huang F. (2013). Stable isotope fractionation by thermal diffusion through partially molten wet and dry silicate rocks. *Earth Planet. Sci. Lett.* **365**, 51-62.

- Bottke W. F., Nesvornyy D., Grimm R. E., Morbidelli A. and O'Brien D. P. (2006) Iron meteorites as remnants of planetesimals formed in the terrestrial planet region. *Nature* **439**, 821-824.
- Buchwald V. F. (1975) Handbook of Iron Meteorites. Univ. California Press.
- Choi B.-G., Ouyang X. and Wasson J. T. (1995) Classification and origin of IAB and III CD iron meteorites. *Geochim. Cosmochim. Acta* **59**, 593-612.
- Ciesla F. J., Davison T. M., Collins G. S. and O'Brien D. P. (2013) Thermal consequences of impacts in the early solar system. *Meteorit. Planet. Sci.* **48**, 2559-2576.
- Clayton R. N. and Mayeda T. K. (1996) Oxygen isotope studies of achondrites. *Geochim. Cosmochim. Acta* **60**, 1999-2017.
- Clayton R. N., Mayeda T. K., Olsen E. J. and Prinz M. (1983) Oxygen isotope relationships in iron meteorites. *Earth Planet. Sci. Lett.* **65**, 229-232.
- Davis, A.M., Ganapathy, R., Grossman, L., 1977. Pontlyfni - A differentiated meteorite related to the group IAB irons. *Earth Planet. Sci. Lett.* **35**, 19-24.
- Davison T. M., Ciesla F. J. and Collins G. S. (2012) Post-impact thermal evolution of porous planetesimals. *Geochim. Cosmochim. Acta* **95**, 252-269.
- Davison T. M., O'Brien D. P., Ciesla F. J. and Collins G. S. (2013) The early impact histories of meteorite parent bodies. *Meteorit. Planet. Sci.* **48**, 1894-1918.
- Day J. M. D., Walker R. J., Ash R. D., Liu Y., Rumble D., Irving A. J., Goodrich C. A., Tait K., McDonough W. F. and Taylor L. A. (2012) Origin of felsic achondrites Graves Nunataks 06128 and 06129, and ultramafic brachinites and brachinite-like achondrites by partial melting of volatile-rich primitive parent bodies. *Geochim. Cosmochim. Acta* **81**, 94-128.
- Dodd R.T. (1981) *Meteorites: A Chemical-Petrologic Synthesis*. Cambridge Univ. Press
- Floss C. and Crozaz G. (1991) Ce anomalies in the LEW85300 eucrite: evidence for REE mobilization during Antarctic weathering. *Earth Planet. Sci. Lett.* **107**, 13-24.

- Floss C., Jolliff B. L., Benedix G. K., Stadermann F. J. and Reid J. (2007) Hammadah al Hamra 193: The first amphibole-bearing winonaite. *Am. Mineral.* **92**, 460-467.
- Floss C., Crozaz G., Jolliff B., Benedix G. and Colton S. (2008) Evolution of the winonaite parent body: Clues from silicate mineral trace element distributions. *Meteorit. Planet. Sci.* **43**, 657-674.
- Ford R. L., Benedix G. K., McCoy T. J. and Rushmer T. (2008) Partial melting of H6 ordinary chondrite Kernouve: Constraints on the effects of reducing conditions on oxidized compositions. *Meteorit. Planet. Sci.* **43**, 1399-1414.
- Gardner-Vandy K. G., Lauretta D. S. and McCoy T. J. (2013) A petrologic, thermodynamic and experimental study of brachinites: Partial melt residues of an R chondrite-like precursor. *Geochim. Cosmochim. Acta* **122**, 36-57.
- Golabek G. J., Bourdon B. and Gerya T. V. (2014) Numerical models of the thermomechanical evolution of planetesimals: Application to the acapulcoite-lodranite parent body. *Meteorit. Planet. Sci.* **49**, 1083-1099.
- Goodrich C. A. and Delaney J. S. (2000) Fe/Mg-Fe/Mn relations of meteorites and primary heterogeneity of primitive achondrite parent bodies. *Geochim. Cosmochim. Acta* **64**, 149-160.
- Grady M. M. and Pillinger C. T. (1986) Carbon Isotope Relationships in Winonaites and Forsterite Chondrites. *Geochim. Cosmochim. Acta* **50**, 255-263.
- Grady M. M., Wright I. P., Carr L. P. and Pillinger C. T. (1986) Compositional differences in enstatite chondrites based on carbon and nitrogen stable isotope measurements. *Geochim. Cosmochim. Acta* **50**, 2799-2813.
- Graham A. L., Easton A. J. and Hutchison R. (1977) Forsterite chondrites; the meteorites Kakangari, Mount Morris (Wisconsin), Pontlyfni, and Winona. *Mineral. Mag.* **41**, 201-210.

- Greenwood R. C., Franchi I. A., Gibson J. M. and Benedix G. K. (2012) Oxygen isotope variation in primitive achondrites: The influence of primordial, asteroidal and terrestrial processes. *Geochim. Cosmochim. Acta* **94**, 146-163.
- Herpfer M. A., Larimer J. W. and Goldstein J. I. (1994) A comparison of metallographic cooling rate methods used in meteorites. *Geochim. Cosmochim. Acta* **58**, 1353-1365.
- Hunt A., Benedix G., Strekopytov S., Unsworth C., Hammond S. and Bland P. A. (2011) The Major and Trace-element Composition of the Winonaites: Evidence for Heterogeneity and Implications for Geochemical Analysis., *Lunar Planet. Sci. XXXXII*. Lunar Planet. Inst., Houston #1809 (abstr.).
- Irving, A.J. and Rumble D. (2006) Oxygen isotopes in Brachina, SAH995555 and Northwest Africa 1054. *Meteorit. Planet. Sci.* **41**, 5288 (abstr.).
- Jarosewich E. (1967) Chemical analyses of 7 stony meteorites and one iron with silicate inclusions. *Geochim. Cosmochim. Acta* **31**, 1103-1106.
- Jarosewich E. (1990) Chemical-analyses of meteorites - A compilation of stony and iron meteorite analyses. *Meteoritics* **25**, 323-337.
- Kelly W.R. and Larimer J.W. (1977) Chemical fractionations in meteorites—VIII. Iron meteorites and the cosmochemical history of the metal phase. *Geochim. Cosmochim. Acta* **41**, 93-111.
- King E. A., Jarosewich E. and Daugherty F. W. (1981) Tierra Blanca: An unusual achondrite from west Texas. *Meteoritics* **16**, 229-237.
- Kracher A. (1974) Untersuchungen am Landes Meteorit. In: Kiesel W. And Mahss H., Jr. (eds.), *Analyse extraterrestrischen Materials*, Springer, 315-326.
- Kruijer, T. S., Kleine, T., Fischer-Gödde, M., Burkhardt, C. & Wieler, R. (2014). Nucleosynthetic W isotope anomalies and the Hf–W chronometry of Ca–Al-rich inclusions. *Earth Planet. Sci. Lett.* **403**, 317-327.
- Kullerud G. (1963) The Fe-Ni-S system. *Ann. Rep. Geophys. Lab.* **67**, 4055–4061.

- Lichtenberg T., Golabek G. J., Gerya T. V., and Meyer M. R. (2016). The effects of short-lived radionuclides and porosity on the early thermo-mechanical evolution of planetesimals. *Icarus* **274**, 350-365.
- Lodders K. (2003) Solar System Abundances and Condensation Temperatures of the Elements. *Astrophys. J.* **591**, 1220-1247.
- Markowski A., Quitte G., Halliday A. N. and Kleine T. (2006) Tungsten isotopic compositions of iron meteorites: Chronological constraints vs. cosmogenic effects. *Earth Planet. Sci. Lett.* **242**, 1-15.
- Mason B. and Jarosewich E. (1967) The Winona meteorite. *Geochim. Cosmochim. Acta* **31**, 1097-1099.
- McCoy T. J., Keil K., Clayton R. N., Mayeda T. K., Bogard D. D., Garrison D. H., Huss G. R., Hutcheon I. D. and Wieler R. (1996) A petrologic, chemical, and isotopic study of Monument Draw and comparison with other acapulcoites: Evidence for formation by incipient partial melting. *Geochim. Cosmochim. Acta* **60**, 2681-2708.
- McCoy T. J., Keil K., Muenow D. W. and Wilson L. (1997a) Partial melting and melt migration in the acapulcoite-lodranite parent body. *Geochim. Cosmochim. Acta* **61**, 639-650.
- McCoy T. J., Keil K., Clayton R. N., Mayeda T. K., Bogard D. D., Garrison D. H. and Wieler R. (1997b) A petrologic and isotopic study of lodranites: Evidence for early formation as partial melt residues from heterogeneous precursors. *Geochim. Cosmochim. Acta* **61**, 623-637.
- McSween H., Bennett M. and Jarosewich E. (1991). The mineralogy of ordinary chondrites and implications for asteroid spectrophotometry. *Icarus* **90**, 107-116.
- Mittlefehldt D. W., McCoy T. J., Goodrich C. A. and Kracher A. (1998) Non-chondritic meteorites from asteroidal bodies, in: Papike, J.J. (Ed.), *Planetary Materials, Reviews in Mineralogy*, Vol 36, pp. 4-1 - 4-196.

- Prinz M., Waggoner D. G. and Hamilton P. J. (1980) Winonaites: A primitive achondritic group related to silicate inclusions in IAB irons, *Lunar Planet. Sci. XI*. Lunar Planet. Inst., Houston, 902-904 (abstr.).
- Prinz M., Nehru C. E., Delaney J. S. and Weisberg M. (1983) Silicates in IAB and III CD irons, winonaites, lodranites and Brachina: A primitive and modified primitive group. *Lunar Planet. Sci. XIV*, Lunar Planet. Inst., Houston, 616-617 (abstr.).
- Qin L., Dauphas N., Wadhwa M., Masarik J. and Janney P. E. (2008) Rapid accretion and differentiation of iron meteorite parent bodies inferred from  $^{182}\text{Hf}$ - $^{182}\text{W}$  chronometry and thermal modeling. *Earth Planet. Sci. Lett.* **273**, 94-104.
- Russell S. S., Zipfel J., Folco L., Jones R., Grady M. M., McCoy T. and Grossman J. N. (2003) The Meteoritical Bulletin, No. 87, 2003 July. *Meteorit. Planet. Sci.* **38**, A189-A248.
- Ruzicka A. and Hutson M. (2010) Comparative petrology of silicates in the Udei Station (IAB) and Miles (IIE) iron meteorites: Implications for the origin of silicate-bearing irons. *Geochim. Cosmochim. Acta* **74**, 394-433.
- Schreiber H. D., Lauer H. V. and Thanyasiri T. (1980) The redox state of cerium in basaltic magmas: an experimental study of iron-cerium interactions in silicate melts. *Geochim. Cosmochim. Acta* **44**, 1599-1612.
- Schulz T., Münker C., Palme H. and Mezger K. (2009) Hf-W chronometry of the IAB iron meteorite parent body. *Earth Planet. Sci. Lett.* **280**, 185-193.
- Schulz T., Münker C., Mezger K. and Palme H. (2010) Hf-W chronometry of primitive achondrites. *Geochim. Cosmochim. Acta* **74**, 1706-1718.
- Schulz T., Upadhyay D., Münker C. and Mezger K. (2012) Formation and exposure history of non-magmatic iron meteorites and winonaites: Clues from Sm and W isotopes. *Geochim. Cosmochim. Acta* **85**, 200-212.

- Stolper E. (1977) Experimental petrology of eucritic meteorites. *Geochim. Cosmochim. Acta* **41**, 587-611.
- Takeda H. (1997) Mineralogical records of early planetary processes on the howardite, eucrite, diogenite parent body with reference to Vesta. *Meteorit. Planet. Sci.* **32**, 841-853.
- Takeda H., Mori H., Hiroi T. and Saito J. (1994) Mineralogy of new Antarctic achondrites with affinity to Lodran and a model of their evolution in an asteroid. *Meteoritics* **29**, 830-842.
- Takeda H., Bogard D. D., Mittlefehldt D. W. and Garrison D. H. (2000) Mineralogy, petrology, chemistry, and Ar-39-Ar-40 and exposure ages of the Caddo County IAB iron: Evidence for early partial melt segregation of a gabbro area rich in plagioclase-diopside. *Geochim. Cosmochim. Acta* **64**, 1311-1327.
- Theis K. J., Schönbächler M., Benedix G. K., Rehkämper M., Andreasen R. and Davies C. (2013) Palladium–silver chronology of IAB iron meteorites. *Earth Planet. Sci. Lett.* **361**, 402-411.
- Touboul M., Kleine T., Bourdon B., Van Orman J. A., Maden C. and Zipfel J. (2009) Hf-W thermochronometry: II. Accretion and thermal history of the acapulcoite-lodranite parent body. *Earth Planet. Sci. Lett.* **284**, 168-178.
- Vogel N. and Renne P. R. (2008)  $^{40}\text{Ar}$ - $^{39}\text{Ar}$  dating of plagioclase grain size separates from silicate inclusions in IAB iron meteorites and implications for the thermochronological evolution of the IAB parent body. *Geochim. Cosmochim. Acta* **72**, 1231-1255.
- Wasson J. T. & Kallemeyn G. W. (1988). Compositions of chondrites. *Phil. Trans. R. Soc. A* **325**, 535-544.
- Wasson J. T., Willis J., Wai C. M. and Kracher A. (1980) Origin of iron meteorite groups IAB and IIICD. *Z. Naturforsch* **35a**, 781-795.

- Wasson J. T. and Kallemeyn G. W. (2002) The IAB iron-meteorite complex: A group, five sub-groups, numerous grouplets, closely related, mainly formed by crystal segregation in rapidly cooling melts. *Geochim. Cosmochim. Acta* **66**, 2445-2473.
- Weisberg M. K., McCoy T. J. and Krot A. N. (2006) Systematics and Evaluation of Meteorite Classification, in *Meteorites and the Early Solar System II* (eds. D.S. Lauretta and H.Y. McSween). The University of Arizona Press, Tucson, AZ, pp. 19-52.
- Wiik H. B. (1956) The chemical composition of some stony meteorites. *Geochim. Cosmochim. Acta* **9**, 279-289.
- Wlotzka F. and Jarosewich E. (1977) Mineralogical and chemical compositions of silicate inclusions in the El Taco, Camp del Cielo, iron meteorite. *Smithsonian Contrib. Earth Sci.* **19**, 104-125.
- Worsham E. A., Bermingham K. R., and Walker R. J. (2016). Siderophile element systematics of IAB complex iron meteorites: New insights into the formation of an enigmatic group. *Geochim. Cosmochim. Acta* **188**, 261-283.
- Yanai K., and Kojima H. (1995) Catalog of Antarctic Meteorites. National Institute of Polar Research, Tokyo, Japan.
- Yugami K., Takeda H., Kojima H. and Miyamoto M. (1998) Modal mineral abundances and the differentiation trends in primitive achondrites. *Antarct. meteorite res.* **11**, 49-70.